Workshop on

Nuclear Reaction Data and Nuclear Reactors: Physics, Design and Safety

13 March - 14 April 2000

Miramare - Trieste, Italy

The Optical Model and ECIS95

Brett Vern Carlson
Instituto Tecnologico de Aeronautica
Sao Jose Dos Campos, Brazil

The Optical Model and ECIS95

B.V. Carlson

Departamento de Física, Instituto Tecnológico da Aeronáutica,
Centro Técnico Aeroespacial, 12228-900 São José dos Campos, SP, Brazil

February 28, 2000

Abstract

The basic features of elastic and inelastic scattering within the framework of the spherical and deformed nuclear optical models are discussed. The calculation of cross sections, angular distributions and other scattering quantities using J. Raynal's code ECIS95 is described. The use of the ECIS method (Equations Couplées en Itérations Séquentielles) in coupled-channels and distorted-wave Born approximation calculations is also reviewed.

1 Introduction

A nuclear reaction is initiated when a nucleon or nucleus collides with another nucleon or nucleus. Reactions are characterized in first place by the incoming nuclei and the outgoing reaction products. Examples of the usual notation for this are $^{14}C(n,n)^{14}C$, for the elastic scattering of neutrons on ^{12}C, $^{56}Fe(p,t)^{54}Fe$, for the pickup by a proton of two neutrons from ^{56}Fe, and $^{235}U(n,n')$ for inelastic neutron scattering from ^{235}U.

A complete description of a nuclear reaction involves other observable quantities beside the incoming nuclei and the outgoing reaction products. Among these are the relative energy of the incoming and outgoing nuclei and the scattering angle of the outgoing products. When the nuclei/nucleons involved have spin and/or excited states, their polarizations and/or excitation energies can also be observed.

The characteristics of the reactions induced by a given pair of incident nucleons/nuclei can be summarized in distributions of the occurrence of the reaction products, called cross sections. Quantitatively, the cross section σ_p for the production of a product p is defined as

$$\sigma_p = \frac{\text{number of particles p produced per unit time}}{\text{number of incident particles per unit time per unit area}}. \tag{1}$$

Cross sections have the dimension of area. The information obtained from cross sections often depends quite strongly on the internal structure of the initial and final nuclei. In fact, the comparison of experimental scattering observables with those obtained from various nuclear models can teach us a great deal about the structure of individual nuclei. After having used such a comparison to determine the model parameters appropriate for a given system, one hopes to use the same parameters to predict cross sections in other energy ranges or in neighboring systems.

1

At low energies and for all but the lightest nuclear systems, nuclear reactions occur on two very distinct time scales. Direct reactions occur promptly, on a time scale of the same magnitude as the time it takes the projectile nucleus to pass by the target nucleus. Compound nuclear reactions, which involve the formation of a quasi-bound intermediate complex, occur on a time scale that is at least several orders of magnitude larger. A naive application of the uncertainty relation, $\Delta E \Delta t \geq \hbar$, would lead one to expect their energy scales to be inversely related. This is, in fact, the case. The contributions of direct reactions to the cross sections vary smoothly with energy. Compound nuclear reactions make contributions to the cross sections that fluctuate rapidly with energy.
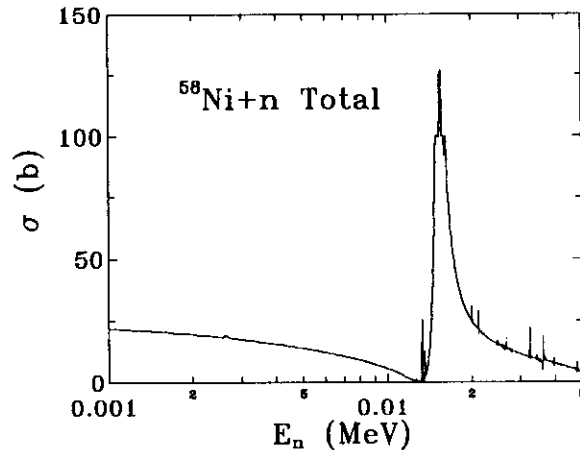

Figure 1: The total cross section for neutrons incident on ^{58}Ni at low incident energy, taken from the data of Ref. 1

The difference in the energy dependence of the direct and compound nucleus contributions to the cross section is clearly seen in Fig. 1, which displays the total neutron cross section on ^{58}Ni at extremely low incident neutron energy. One observes a direct reaction cross section – the result of elastic scattering of the neutron, in this case – that varies slowly with energy, except where it is punctuated by a faster variation due to the presence of a compound nuclear state of ^{59}Ni of about the same energy. At such low energies, separation of the direct and compound nucleus cross sections is a fairly straightforward (although often grueling) task.

At higher energies, the density of compound nucleus states becomes so large that the individual contributions can no longer be resolved. It then becomes impossible to distinguish the slow energy dependence of the direct contribution from the rapid variations of the compound nucleus one. An example of this is given in Fig. 2, where the total cross section for neutrons incident on ^{58}Ni is again shown, but now at higher energies. The fluctuations in the cross section, called Ericson fluctuations,[3] do not permit the determination of the contribution to the cross section of each individual compound nuclear state. Instead, only the average properties of the compound nucleus contribution to the cross section can be determined. It is in this context that the optical potential plays a crucial role in the separation of the two contributions.

The principal objective of the optical model is to describe just the prompt, direct reactions
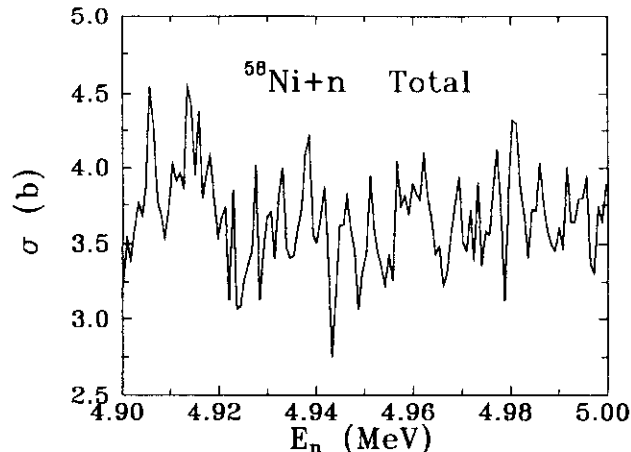
2

Figure 2: The total cross section for neutrons incident on ^{58}Ni in a small incident energy range close to 5 MeV, taken from the data of Ref. 2

in a nuclear collision. To separate the direct reactions from the compound-nucleus ones (theoretically), one assumes that the compound-nucleus reactions do not contribute to the average wave function and scattering amplitudes, due to their rapid fluctuations in energy. Note that the compound-nucleus reactions still DO contribute to the average cross sections, which are, for the most part, proportional to the squares of the amplitudes. The energy-averaged amplitudes, however, are associated with the scattering amplitudes for the prompt component of the scattering. The optical model potential is defined as the potential which furnishes the energy-averaged scattering amplitudes.

In a wider context, the optical potential can be considered an effective potential that takes into account all of the physical processes one does not want to take into account explicitly. The most important of these are the rapidly fluctuating compound-nucleus contributions to the scattering. But direct processes are also included at times. One example of this is the use of an effective spherical optical model potential to take into account the coupling to excited states of the target. Another example is the deuteron optical potential, which usually contains the contribution of direct deuteron breakup.

As well as being fundamental for the calculation of direct reaction observables, optical model calculations are also used to produce the transmission coefficients essential for the analysis of compound nucleus cross sections within the Hauser-Feshbach statistical theory. They are thus one of the first and most important steps in the evaluation of nuclear cross sections.

2 Formal development of the optical model

To derive the optical model from 'first principles', one begins by partitioning the Hilbert space of states into a component $\mathcal{P}$ containing the prompt states and an orthogonal component $\mathcal{Q}$ that contains the closed channels of the intermediate compound complex.[4] As a concrete example, one may consider $\mathcal{P}$ to be the subspace consisting of a nucleon scattering on ^{58}Ni, while $\mathcal{Q}$ consists

of the ground and excited states of the nucleus ^{59}Ni (and other processes, such as γ emission, that have been neglected). The projection operators, P and Q, onto the subspaces $\mathcal{P}$ and $\mathcal{Q}$, respectively, which satisfy the properties

$$P = P^\dagger \qquad Q = Q^\dagger$$
$$P^2 = P \qquad Q^2 = Q \tag{2}$$
$$P + Q = 1 \,,$$

are then used to decompose the state vector of the system, Ψ, and the Schrödinger equation it satisfies,

$$(E - H)\Psi = 0 \,. \tag{3}$$

The prompt component of the state vector is $P\Psi$, while the slower component is $Q\Psi$, with

$$\Psi = P\Psi + Q\Psi \,. \tag{4}$$

We can multiply the Schrödinger equation on the left by P or by Q and use the decomposition of the wave vector to write the equation as two coupled equations,

$$(E - H_{PP})P\Psi = V_{PQ}Q\Psi \tag{5}$$

and

$$(E - H_{QQ})Q\Psi = V_{QP}P\Psi \,, \tag{6}$$

where

$$H_{PP} \equiv H_{0P} + V_{PP} \equiv PH_0P + PVP, \qquad V_{PQ} \equiv PHQ, \qquad \text{etc.,}$$

and we have assumed that the contributions to the Hamiltonian of the internal degrees of freedom and the kinetic energy, both contained in H_0, do not couple the $\mathcal{P}$ and $\mathcal{Q}$ subspaces. We may formally solve the first of these, Eq.(5), as

$$P\Psi_i = \phi_i^{(+)} + \frac{1}{E^{(+)} - H_{PP}}V_{PQ}Q\Psi_i \,, \tag{7}$$

in which the $(+)$ denotes an incoming wave boundary condition, the vector $\phi_i^{(+)}$ satisfies the Schrödinger equation in the $\mathcal{P}$ subspace,

$$(E - H_{PP})\phi_i^{(+)} = 0 \,, \tag{8}$$

with an incoming wave in channel i alone (and none in the $\mathcal{Q}$ subspace) and $P\Psi_i$ and $Q\Psi_i$ are the components of the full wave vector that evolve from this incoming wave. The solution $P\Psi_i$, when substituted into the second coupled equation, Eq. (6), yields

$$(E - H_{QQ} - W_{QQ})Q\Psi_i = V_{QP}\phi_i^{(+)} \,, \tag{9}$$

4

where

$$W_{QQ} \equiv V_{QP} \frac{1}{E^{(+)} - H_{PP}} V_{PQ} \,. \tag{10}$$

We can decompose the $\mathcal{P}$-subspace Greens function into its real and imaginary parts as

$$\frac{1}{E^{(+)} - H_{PP}} = \frac{P.P.}{E - H_{PP}} - i\pi\delta(E - H_{PP}) \,, \tag{11}$$

where $P.P.$ represents the principal part. The open channels in the $\mathcal{P}$ subspace thus make a negative imaginary contribution to W_{QQ}, which results in singularities in the wave vector in the lower half of the complex E plane.

Eq. (9) can be solved to obtain the $\mathcal{Q}$-subspace component of the wave vector as

$$Q\Psi_i = \frac{1}{E - H_{QQ} - W_{QQ}} V_{QP} \phi_i^{(+)} \,, \tag{12}$$

which then permits the expression of the $\mathcal{P}$-subspace component of the wave vector as

$$P\Psi_i = \phi_i^{(+)} + \frac{1}{E^{(+)} - H_{PP}} V_{PQ} \frac{1}{E - H_{QQ} - W_{QQ}} V_{QP} \phi_i^{(+)} \,. \tag{13}$$

A careful analysis of the last expression leads one to the scattering matrix $\mathcal{T}_{fi}$ giving the transition amplitude in the $\mathcal{P}$ subspace,

$$\mathcal{T}_{fi} = \mathcal{T}_{fi}^{(P)} + \left\langle \phi_f^{(-)} \left| V_{PQ} \frac{1}{E - H_{QQ} - W_{QQ}} V_{QP} \right| \phi_i^{(+)} \right\rangle \,. \tag{14}$$

The first term in this expression is the direct scattering amplitude associated with scattering in the $\mathcal{P}$ subspace alone. The second term describes the slower processes that result from coupling through the states of the $\mathcal{Q}$ subspace. The first term varies slowly as a function of energy while the second term varies rapidly.

The energy average of the $\mathcal{P}$-subspace wave vector can now be written as

$$\langle P\Psi_i \rangle = \phi_i^{(+)} + \frac{1}{E^{(+)} - H_{PP}} V_{PQ} \left\langle \frac{1}{e_{QQ}} \right\rangle V_{QP} \phi_i^{(+)} \,, \tag{15}$$

where

$$e_{QQ} = E - H_{QQ} - W_{QQ} \tag{16}$$

is the only rapidly varying function of the energy in the expression. The average wave vector can be written in a Schrödinger-equation-like form by multiplying both sides of the expression, Eq. (15), by $E^{(+)} - H_{PP}$,

$$(E - H_{PP}) \langle P\Psi_i \rangle = V_{PQ} \left\langle \frac{1}{e_{QQ}} \right\rangle V_{QP} \phi_i^{(+)} \,. \tag{17}$$

Using Eq. (15) again to rewrite the wave vector $\phi_i^{(+)}$ as

$$\phi_i^{(+)} = \frac{1}{1 + (E^{(+)} - H_{PP})^{-1} V_{PQ} \langle 1/e_{QQ} \rangle V_{QP}} \langle P\Psi_i \rangle \,, \tag{18}$$

5

substituting this in Eq. (17) and performing a bit of algebra, one finally obtains the optical model equation,

$$\left[E - H_{PP} - V_{PQ} \frac{1}{\langle 1/e_{QQ} \rangle^{-1} + W_{QQ}} V_{QP} \right] \langle P\Psi_i \rangle = 0 \,.$$ (19)

The optical potential can thus be written as

$$V_{opt} = V_{PP} + V_{PQ} \frac{1}{\langle 1/e_{QQ} \rangle^{-1} + W_{QQ}} V_{QP} \,.$$ (20)

To conclude the formal development of the optical model, one must evaluate the average value $\langle 1/e_{QQ} \rangle$. The simplest way of doing this is to average the quantity $1/e_{QQ}$ over a normalized Lorentzian density,

$$\left\langle \frac{1}{e_{QQ}} \right\rangle = \int dE_0 \, \frac{\rho(E, E_0)}{E_0 - H_{QQ} - W_{QQ}} \,,$$ (21)

where

$$\rho(E, E_0) = \frac{\Delta}{2\pi} \frac{1}{(E - E_0)^2 + (\Delta/2)^2} \,.$$ (22)

Assuming the quantity $1/e_{QQ}$ to have no poles in the upper half of the complex E plane (due to causality, it should have them only in the lower half-plane), we can perform the integral by closing the contour and calculating residues in the upper half plane to obtain

$$\left\langle \frac{1}{e_{QQ}} \right\rangle = \frac{1}{E + i\Delta/2 - H_{QQ} - W_{QQ}} \,,$$ (23)

and hence

$$V_{opt} = V_{PP} + V_{PQ} \frac{1}{E - H_{QQ} + i\Delta/2} V_{QP} \,.$$ (24)

The optical potential is obviously energy-dependent, non-local and complex due to the energy-averaged propagator $(E - H_{QQ} + i\Delta/2)^{-1}$ in the second term. Its imaginary part is negative, resulting in a potential that is absorptive. The flux of particles leaving the scattering region is, in this case, smaller than the incident flux, with the remaining fraction of the flux being absorbed by the potential. It is through its imaginary part that the optical potential takes into account the flux that is lost from the states of the $\mathcal{P}$ subspace to the states of the $\mathcal{Q}$ subspace.

The optical scattering matrix can easily be derived in the same manner. One obtains

$$\langle \mathcal{T} \rangle_{fi} = \mathcal{T}_{fi}^{(P)} + \left\langle \phi_f^{(-)} \left| V_{PQ} \left\langle \frac{1}{e_{QQ}} \right\rangle V_{QP} \right| \phi_i^{(+)} \right\rangle \,,$$ (25)

with $\langle 1/e_{QQ} \rangle$ given by Eq. (23). Observe that the second, rapidly fluctuating term does not vanish completely. Indeed it should not vanish in general, for its average contribution describes the loss of flux from the prompt channels to the long-lived compound-nucleus states.

3 Low-energy neutron scattering

At low relative energies, a collision between charged nuclei or a nucleus and a charged nucleon is dominated by the Coulomb force, which keeps the two beyond the range of nuclear interaction. Only neutrons can enter sufficiently close to a nucleus at such energies to feel the effects of the nuclear force.

Several factors also simplify the description of low-energy neutron scattering. The centripetal barrier keeps all but the l=0 s-wave contribution effectively out of the reach of the nuclear interaction for energies greater than about 50 keV. In addition, with few exceptions, nuclei have no excited states at energies lower than about 20 keV. The prompt component of neutron scattering then reduces to s-wave elastic scattering in this energy range.

The optical model equation for the s-state wave function ψ_0 is

$$(E_{cm} - T - U_{opt})\frac{\psi_0}{r} = 0,\tag{26}$$

which can be reduced to

$$\frac{d^2\psi_0}{dr^2} + \left[k^2 - \frac{2\mu}{\hbar^2}U_{opt}\right]\psi_0 = 0,\tag{27}$$

where the wavenumber is $k = \sqrt{2\mu E_{cm}/\hbar^2}$, μ is the reduced mass and E_{cm} the center-of-mass energy.

To solve this equation numerically, one develops the solution, $\psi_{0,int}(r)$, starting from $r = 0$, using the condition that the wave function vanishes at the origin, $\psi_{0,int}(r = 0) = 0$ and one of many possible numerical methods (Cowell, Numerov, modified Numerov, Runge-Kutta, etc.). The equation is solved numerically out to a radius r_m, beyond which the optical potential can be neglected. For values of the radius equal to or larger than this matching radius, the solution to the differential equation that satisfies the incoming wave boundary condition takes the form

$$\psi_{0,ext}(r) = \frac{i}{2}(e^{-ikr} - S_0 e^{ikr}) \qquad r \geq r_m.\tag{28}$$

One requires, at the matching radius r_m, that this external wave function and its derivative be the continuous extensions of the numerical wave function obtained in the the internal region and of its derivative. This results in two equations,

$$a_0\psi_{0,int}(r_m) = \frac{i}{2}(e^{-ikr_m} - S_0 e^{ikr_m})\tag{29}$$

and

$$a_0\frac{d}{dr}\psi_{0,int}(r_m) = \frac{k}{2}(e^{-ikr_m} + S_0 e^{ikr_m}),\tag{30}$$

whose solution yields the amplitude of the internal wave function, a_0, and the S-matrix element, S_0.

Once the S-matrix is known, the cross sections can be calculated. For the case of s-wave scattering, these are

$$\sigma_{tot} = \frac{2\pi}{k^2}(1 - \operatorname{Re} S_0),$$

$$\sigma_{el} = \frac{\pi}{k^2}|S_0 - 1|^2,$$

$$\text{and} \quad \sigma_r = \frac{\pi}{k^2}(1 - |S_0|^2) = \frac{\pi}{k^2}T_0, \tag{31}$$

where T_0 is the s-wave transmission coefficient. The reaction cross section and the transmission coefficient T_0 are non-zero when the S-matrix element S_0 is smaller than one in magnitude. This occurs when flux is absorbed by the long-lived compound-nucleus states. Care must be taken, however, when comparing the optical model reaction cross section to the experimental one. A part of the flux absorbed by the compound nucleus can later be re-emitted in the elastic channel, in which case it should rightly be considered part of the elastic cross section.

Of the three cross sections, only the total one can be compared directly with experimental data, as it is the only one that is linear in the scattering amplitude (here the S-matrix element S_0). The S-matrix element can be written in general as the sum of an average and a fluctuating part, $S = S_{ave} + S_{fl}$. The average elastic cross section then has the form

$$\langle \sigma_{el} \rangle = \frac{\pi}{k^2}|S_{ave} - 1|^2 + \frac{\pi}{k^2}\left\langle |S_{fl}|^2 \right\rangle. \tag{32}$$

The first term alone gives the elastic cross section of the optical model. The second term contributes to the optical model reaction cross section.

Other scattering quantities of physical interest can also be calculated for low-energy neutron scattering. At extremely low energies — below the resonance region — the elastic cross section is observed to approach a constant value, σ_{el}^0. This value is used to calculate the scattering radius, $R' = \sqrt{\sigma_{el}^0/4\pi}$.

In the resonance region, s-wave and p-wave strength functions can be defined. The s-wave strength function, s_0, relates the average neutron partial width $\langle \Gamma_0 \rangle$ and spacing D_0 of the resonances to the optical model absorption. One has, approximately,

$$s_0 = \frac{\langle \Gamma_0 \rangle}{D_0}\left(\frac{E_0}{E_{cm}}\right)^{1/2} \approx \frac{1 - |S_0|^2}{2\pi\sqrt{E_{cm}}}, \tag{33}$$

where E_0 is usually taken to be 1 eV. The factor $\sqrt{E_{cm}}$, the s-wave penetrability, cancels the energy dependence of the neutron partial width, so that the strength function varies slowly with the incident neutron energy. The p-wave strength function, s_1, relating the average partial width and spacing of the $l = 1$ reonances is defined analogously in terms of the p-wave S-matrix elements and penetrability.

Adjustment of the optical model parameters at low energy to reproduce the s-wave and p-wave strength functions, the scattering radius and the total cross section is known as the SPRT method.[5] A good fit to these observables is important in determining the low energy behavior of the optical cross sections and the transmission coefficients, which is important, in turn, in determining the behavior of compound nucleus cross section calculations near threshold.

8

4   The phenomenological optical potential

The formal derivation of the optical potential presented in Section 2 might suggest that it could be calculated directly. Although a good deal of work has indeed been done in this direction, the resulting potentials are often difficult to calculate and still not sufficiently precise. They also have the drawback of being non-local, which can greatly complicate solution of the corresponding Schrödinger equation.[6, 7, 8]

Instead, phenomenological optical model potentials are normally used to compare and fit to experimental data. With few exceptions, these potentials are taken to be local. However, the qualitative characteristics of the geometry and the general trend of the energy dependence of the phenomenological potentials are quite similar to those found in microscopic potentials. Both types of potentials are, after all, trying to describe the same physical processes.

In the empirical potentials, the functional form is usually determined by a limited set of parameters that are adjusted to obtain a best fit with the experimental data. Over the years, a standard form of the phenomenological optical model potential has evolved, which permits the parametrization of the scattering of a light particle (neutron, proton, deuteron, triton, ^{3}He or alpha) from a given nucleus. This is

$$
U_{opt}(r) =
\begin{array}{ll}
+V_C(r) & \text{a Coulomb term,} \\
-V\, f_V(r) & \text{a real volume term,} \\
+V_s g_V(r) & \text{a real surface term,} \\
-iW_s\, g_W(r) & \text{an imaginary surface term,} \\
-iW_v\, f_W(r) & \text{an imaginary volume term,} \\
-d_{so}\, \vec{l} \cdot \vec{s}\, V_{so}\, h_{V_{so}}(r) & \text{a real spin-orbit term,} \\
+i d_{so}\, \vec{l} \cdot \vec{s}\, W_{so}\, h_{W_{so}}(r) & \text{and an imaginary spin-orbit term,}
\end{array}
\tag{34}
$$

where the spin-orbit constant is $d_{so} = (\hbar/m_\pi c)^2 \approx 2$ fm^2, m_π being the pion mass.

The Coulomb term is usually taken to be the interaction of a point charge with a uniformly charged sphere of radius R_c,

$$
V_C(r) = \left\{
\begin{array}{ll}
\left(\frac{3}{2} - \frac{r^2}{2R_c^2}\right) Z_p Z_t e^2 / R_c & r \le R_c \\
Z_p Z_t e^2 / r & r > R_c
\end{array}
\right.
\tag{35}
$$

where Z_p and Z_t are the projectile and target charge, respectively. Although this potential neglects the surface diffusivity of the nuclear charge distribution, it is a reasonable approximation in the case of the scattering of light particles from nuclei.

The real and imaginary volume terms are normally taken to be of Wood-Saxon form,

$$
f_i = \frac{1}{1 + \exp\left[(r - R_i)/a_i\right]} \qquad i = V, W\,,
\tag{36}
$$

where R_i and a_i are the radii and the diffusivities, respectively, of the two terms. The Wood-Saxon form factor, shown in Fig. 3, can be thought of as a smoothed step function, falling from one for values of the radius r smaller than the radius R_i to zero for values of r greater than R_i, in a few multiples of the diffusivity a_i.
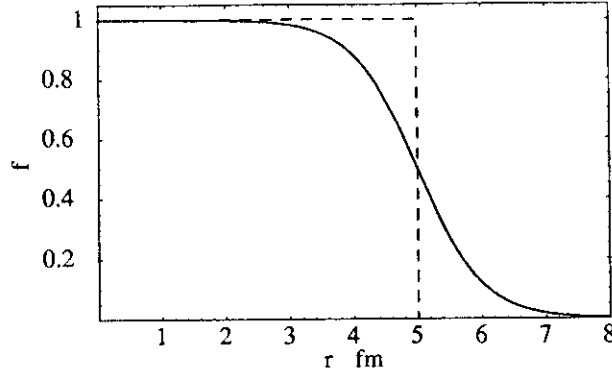
9

Figure 3: The Wood-Saxon (solid line) and sharp cutoff (dashed line) form factors with a radius of R=5 fm and a diffusivity of a=0.5 fm are shown.

The real volume potential reflects the average interaction of the projectile with the nucleons of the target nucleus. The Wood-Saxon form factor it uses is quite similar in form to the nucleon density of a saturated nucleus ($A \geq 30$). (For lighter nuclei, a Gaussian geometry is sometimes used.) The strength of the real volume potential is roughly proportional to the mass of the projectile and decreases with the incident energy, in qualitative agreement with the results of calculations of the nuclear mean field.[9]

The imaginary volume potential takes into account the loss of projectile particles due to collisions with the nucleons of the target. It is zero at low energies, for which the projectile does not have sufficient energy to knock out a target nucleon. At higher energies, it increases slowly with the incident energy, as the phase space available for nucleon knockout increases. At even higher energies, both the real and imaginary volume potentials for nucleon scattering are fairly well described by the impulse approximation, in which the the target density is simply folded with the nucleon-nucleon cross section.[10, 11]

The real and imaginary surface terms of the optical potential are taken to be either the derivative of a Wood-Saxon,

$$g_i(r) = -4a_i \frac{d}{dr} f_i(r) = 4 \frac{\exp\left[(r - R_i)/a_i\right]}{\left(1 + \exp\left[(r - R_i)/a_i\right]\right)^2} \qquad i = V, W, \tag{37}$$

or a Gaussian,

$$g_i(r) = \exp\left[\frac{(r - R_i)^2}{a_i^2}\right] \qquad i = V, W. \tag{38}$$

In either case, the potential peaks at a radius R_i and falls to zero within a few multiples of the diffusivity a_i. A derivative Wood-Saxon form factor with diffusivity a_{WS} is almost indistinguishable from a Gaussian form factor with diffusivity $a_G = 2.21a_{WS}$, as shown in Fig. 4. The code ECIS95 uses only the Wood-Saxon derivative form.

The imaginary surface term of the optical potential takes into account the absorption due to the coupling to the quasi-bound compound nucleus states and to the excitation of low-energy
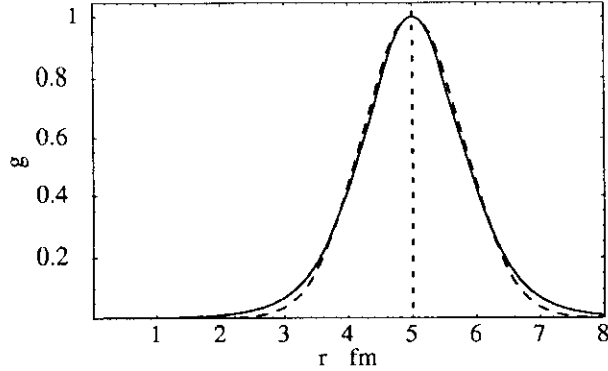
10

Figure 4: The derivative Wood-Saxon (solid line) and Gaussian (dashed line) form factors with a radius of R=5 fm and diffusivities of a_{WS}=0.5 fm. and a_G=1.105 fm, respectively, are shown.

collective modes, which have their couplings concentrated in the nuclear surface. Similar many-body effects can also be invoked to justify the presence of a real surface term. However, given the imaginary surface term, the existence of the real term can be shown to follow directly, by using a dispersion relation based on the causality of the optical potential (no singularities in the energy upper halfplane).[12] The dispersion relation shows that an energy-dependent imaginary potential $W(r, E)$ necessarily leads to a contribution $\Delta V(r, E)$ to the real potential given by

$$\Delta V(r, E) = \frac{P.P.}{\pi} \int_{-\infty}^{\infty} \frac{W(r, E')}{E' - E} dE' . \tag{39}$$

Obviously, if the imaginary term is a surface one, the real term resulting from the dispersion relation will be a surface one as well.

Both the real and imaginary spin-orbit terms of the optical potential are taken to have a Thomas form factor,

$$h_i(r) = -\frac{1}{r} \frac{d}{dr} f_i(r) = \frac{1}{ra_i} \frac{\exp[(r - R_i)/a_i]}{(1 + \exp[(r - R_i)/a_i])^2} \qquad i = V_{so}, W_{so} . \tag{40}$$

Like the surface imaginary term, the Thomas form factor, shown in Fig. 5, yields potentials which peak at a radius near R_i and fall to zero in a few multiples of the diffusivity a_i.

The Thomas form factor, as well as the spin-orbit potential itself, can be derived (for spin 1/2 particles) by performing a reduction of a Dirac equation with Wood-Saxon potentials to an equivalent Schrödinger equation.[9] The spin-orbit interaction and the Thomas form factor can then be interpreted as but another manifestation of the volume interaction of the incident particle with the nucleons of the target nucleus.

The phenomenological optical potential is thus parametrized in terms of a set of potential strengths and corresponding geometrical parameters. These parameters have been adjusted for many systems and values of the relative energy. Several attempts have been made to adjust a single set of parameters to a wide range of systems by introducing a dependence on the target charge and mass as well as that on the relative energy. The potentials obtained using such sets
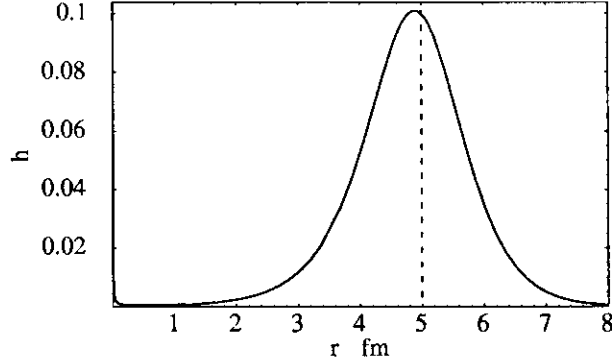
11

Figure 5: The Thomas form factor with a radius of R=5 fm and a diffusivity of a=0.5 fm is shown.

of parameters are called global optical potentials. Many individual and global optical parameter sets can be found in an old compilation by Perey and Perey.[13] However, the best modern reference for optical potential parameters is the Reference Input Parameter Library (RIPL), available both online and in CD from the Internationational Atomic Energy Agency.[14]

For nucleons, typical values of the potential strengths are

$$
\begin{aligned}
V &\approx \quad (45\text{--}55)\text{MeV-}(0.2\text{--}0.3)E\,, \\
W_s &\approx \quad (2\text{--}7)\text{MeV+}(0.3\text{--}0.5)E \qquad\qquad E < 8\text{--}10\text{MeV}, \\
V_{so} &\approx \quad (4\text{--}10)\text{MeV}.
\end{aligned}
\tag{41}
$$

Above 8 – 10 MeV, W_s is usually constant or slightly decreasing. V_s and W_{so} can normally be taken to be zero as can W below about 10 MeV. Above about 10 MeV, W is constant or slightly increasing. As mentioned above, for heavier particles, the real volume potential V scales approximately linearly with the mass.

The radii R_i characteristically take on values close to that of the radius of the target matter distribution. They are often parameterized in terms of reduced radii r_i and the target mass as $R_i = r_i A_t^{1/3}$, with the reduced radii in the range $r_i \approx 1.2$ - 1.3 fm. The diffusivities normally take on values in the range $a_i \approx 0.4$ - 0.7 fm, except in the case of a Gaussian surface form factor, for which the typical values are slightly larger.

Not all of the optical model parameters are uniquely determined by the experimental data. It has been observed, for example, that fairly wide ranges of the parameters V, R_v, W_s, and a_s result in equally good fits to the experimental data if the values of VR_v^2 and $W_s a_s$ remain constant. These are known as potential ambiguities.

5   Partial wave expansion in the single-channel optical model

When angular momenta greater than the s-wave contribute to the scattering, the wave function and the scattering matrix are determined most conveniently when decomposed in angular momentum partial waves.

The partial wave expansion of the scattering wave function of a particle of spin s [15] can be written as

$$\Psi = \frac{4\pi}{kr} \sum_{ljn} i^l\, e^{i\sigma_l} \psi_l^j(r) \mathcal{Y}_{ls}^{jn}(\hat{r}) \mathcal{Y}_{ls}^{jn\dagger}(\hat{k}) , \qquad (42)$$

in terms of the spin-angular functions

$$\mathcal{Y}_{ls}^{jn}(\hat{r}) = i^l \sum_{m\nu} \langle s\nu lm | jn \rangle Y_{lm}(\hat{r}) | s\nu \rangle , \qquad (43)$$

where l and j are the orbital and total angular momenta and $|s\nu\rangle$ is an eigenvector of the particle spin. In the expansion of the wave function, σ_l is the Coulomb phase, $\hat{r}$ denotes the angular variables and $\hat{k}$ the direction of the incident momentum. (The S-matrix element in partial wave l for pure Coulomb scattering of the projectile from the target would be $e^{2i\sigma_l}$.) The factor $i^l e^{i\sigma_l} \psi_l^j(r)/kr$ could have been written as simply $\psi_l^j(r)$ in the partial wave expansion. The form used above simplifies later manipulations.

When the partial-wave expansion of the wave function is substituted in the optical Schrödinger equation, one can extract an independent equation for the wave function ψ_l^j in each partial wave. One finds

$$\left\{ \frac{d^2}{dr^2} - \frac{l(l+1)}{r^2} + k^2 - \frac{2\mu}{\hbar^2} \left(U_{cen}(r) + d_l^j\, U_{so}(r) \right) \right\} \psi_l^j(r) = 0 , \qquad (44)$$

where the spin-orbit constant is $d_l^j = d_{so}\,(j(j+1) - l(l+1) - s(s+1))/2$ and U_{cen} and U_{so} are the central and spin-orbit terms of the phenomenological optical model potential discussed in the previous section.

The incoming-wave boundary condition requires that asymptotically the wave function take the form of an incoming plane wave and an outgoing scattering wave,

$$\Psi \rightarrow \exp\left(i\vec{k}\cdot\vec{r} + i\eta \log(kr - \vec{k}\cdot\vec{r}) \right) \sum_\nu |s\nu\rangle \langle s\nu| \qquad (45)$$

$$+ \frac{1}{r}\exp\left(ikr - i\eta \log(2kr) \right) \sum_{\nu\nu'} |s\nu'\rangle f_{\nu'\nu}(\theta) \langle s\nu| ,$$

where the $f_{\nu'\nu}(\theta)$ are the spin-projected matrix elements of the elastic scattering amplitude and η is the Coulomb parameter, $\eta = \mu Z_p Z_t e^2 / \hbar^2 k$. To be consistent with this expression and satisfy the differential equation, the wave function ψ_l^j must have the asymptotic form,

$$\psi_l^j(r) \rightarrow F_l(r) + (G_l(r) + iF_l(r))\, C_l^j = \frac{i}{2}\left(H_l^-(r) - H_l^+(r) e^{2i\sigma_l} S_l^j \right) e^{-i\sigma_l} , \qquad (46)$$

where $C_l^j = (S_l^j - 1)/2i$, F_l and G_l are the regular and irregular Coulomb wave functions, respectively, and $H_l^\pm = e^{\mp i\sigma_l}(G_l \pm iF_l)$ are the linear combinations of these that asymptotically contain only incoming (H_l^-) or outgoing (H_l^+) waves. S_l^j is the nuclear part of the S-matrix element and $e^{2i\sigma_l}$ the Coulomb part.

The S-matrix elements, S_l^j, are obtained in the same manner as S_0 is obtained in the case of low-energy neutron scattering. In the internal region, the differential equation for each partial

13

wave, Eq. (44), is solved numerically out to the radius, r_m. The numerical solution and its derivative are matched there to the wave function in the external region, given by Eq. (46), and to its derivative, to obtain the ampitude in the internal region, a_l^j, and the S-matrix element, S_l^j.

The only novelty to the solution here is deciding with which partial wave to stop the calculation, for l and j extend to infinity. The calculation is normally stopped when the nuclear S-matrix elements are sufficiently close to one. This occurs when the centripetal barrier no longer permits the projectile to enter the range of nuclear interaction with the target. For partial waves of larger l, the scattering reduces to pure Coulomb scattering (or for neutrons, no scattering at all), as is evident from Eq. (46).

When the asymptotic form of the partial wave function, ψ_l^j, of Eq. (46), is substituted in the partial wave expansion of the total wave function, Eq. (42), and the result is compared to the expected form of the asymptotic wave function, Eq. (45), one can extract the partial wave expansion of the scattering amplitude,

$$f(\theta) = \frac{4\pi}{2ik} \sum_{ljn} \left(e^{2i\sigma_l} S_l^j - 1 \right) \mathcal{Y}_{ls}^{jn}(\hat{r}) \mathcal{Y}_{ls}^{jn\dagger}(\hat{k}), \tag{47}$$

or, in terms of its spin-projected matrix elements,

$$f_{\nu'\nu}(\theta) = \frac{4\pi}{2ik} \sum_{\substack{ljn \\ mm'}} \left(e^{2i\sigma_l} S_l^j - 1 \right) Y_{lm'}(\hat{r}) Y_{lm}^*(\hat{k}) \langle lm's\nu'|jn \rangle \langle jn|lms\nu \rangle . \tag{48}$$

Due to the slow convergence of the Coulomb term, it is convenient to write these amplitudes in a form in which the Coulomb contribution has been summed exactly,

$$\begin{aligned}
f_{\nu'\nu}(\theta) &= \frac{4\pi}{2ik} \sum_{\substack{ljn \\ mm'}} \left[\left(e^{2i\sigma_l} - 1 \right) + e^{2i\sigma_l} \left(S_l^j - 1 \right) \right] Y_{lm'}(\hat{r}) Y_{lm}^*(\hat{k}) \\
&\qquad \times \langle lm's\nu'|jn \rangle \langle jn|lms\nu \rangle \\
\\
&= \delta_{\nu'\nu} f_C(\theta) + \frac{4\pi}{2ik} \sum_{\substack{ljn \\ mm'}} e^{2i\sigma_l} \left(S_l^j - 1 \right) Y_{lm'}(\hat{r}) Y_{lm}^*(\hat{k}) \tag{49} \\
&\qquad \times \langle lm's\nu'|jn \rangle \langle jn|lms\nu \rangle ,
\end{aligned}$$

where

$$f_C(\theta) = -\frac{\eta}{2k \sin^2 \theta/2} \exp \left[-i\eta \log \left(\sin^2 \theta/2 \right) + 2i\sigma_0 \right] \tag{50}$$

is the Coulomb amplitude.

For spin-0 particles, there is only one amplitude. This is

$$f(\theta) = f_{00}(\theta) = f_C(\theta) + \frac{1}{2ik} \sum_l (2l+1) e^{2i\sigma_l} (S_l^l - 1) P_l(\cos\theta). \tag{51}$$

For spin-1/2 particles there are two distinct amplitudes. They are

$$\begin{aligned}
A(\theta) &= f_{\frac{1}{2}\frac{1}{2}} = f_{-\frac{1}{2}-\frac{1}{2}} \tag{52} \\
&= f_C(\theta) + \frac{1}{2ik} \sum_l e^{2i\sigma_l} \left[(l+1)(S_l^{l+\frac{1}{2}} - 1) + l(S_l^{l-\frac{1}{2}} - 1) \right] P_l(\cos\theta).
\end{aligned}$$

14

and

$$B(\theta) \;=\; f_{\frac{1}{2}-\frac{1}{2}} = f_{-\frac{1}{2}\frac{1}{2}} \tag{53}$$

$$= \; \frac{1}{2ik} \sum_l e^{2i\sigma_l} \left[S_l^{l+\frac{1}{2}} - S_l^{l-\frac{1}{2}} \right] P_l^1(\cos\theta) \,.$$

The differential elastic cross section for an unpolarized incident beam is obtained by averaging the squared magnitude of the scattering amplitudes over the initial values of the projectile spin and summing over the final ones. The general expression that results is

$$\frac{d\sigma}{d\Omega} = \frac{1}{2s+1} \sum_{\nu\nu'} |f_{\nu'\nu}(\theta)|^2 \,. \tag{54}$$

For spin-0 particles, this is

$$\frac{d\sigma}{d\Omega} = |f(\theta)|^2 \qquad s = 0\,. \tag{55}$$

For spin-1/2 particles, it is

$$\frac{d\sigma}{d\Omega} = |A(\theta)|^2 + |B(\theta)|^2 \qquad s = 1/2\,. \tag{56}$$

For particles of spin-1/2 and greater, one can define vector and tensor spin observables in terms of other combinations of the amplitudes. In particular, for particles of spin-1/2, the vector polarization, $P(\theta)$, is

$$P(\theta) = \frac{2\,\mathrm{Im}\,A^*(\theta)B(\theta)}{d\sigma/d\Omega}\,. \tag{57}$$

The fraction of flux absorbed from each partial wave is given by the transmission coefficient, T_l^j, defined as

$$T_l^j = 1 - \left| S_l^j \right|^2\,. \tag{58}$$

When the S-matrix element is unitary, no flux is absorbed and the transmission coefficient is zero. When absorption is complete, the transmission coefficient is one. These quantities are essential for calculating statistical reaction cross sections. Quite often, optical model calculations are a mere preliminary to statistical model calculations and are performed only to obtain the transmission coefficients.

The total flux lost in the scattering is related to the reaction cross section through the equation

$$\sigma_r = -\frac{1}{v} \oint \vec{\jmath}\cdot d\vec{a}\,, \tag{59}$$

where it is understood that the probability current,

$$\vec{\jmath} = \frac{\hbar}{2i\mu} \left(\Psi^\dagger \nabla\Psi - (\nabla\Psi^\dagger)\Psi \right)\,, \tag{60}$$

15

is integrated over a surface which tends to infinity. The reaction cross section can be expressed in terms of the transmission coefficients as

$$\sigma_r = \frac{1}{2s+1} \frac{\pi}{k^2} \sum_{lj} (2j+1) T_l^j \, . \tag{61}$$

For charged particles, integration of the differential elastic cross section of Eq. (54) leads to an infinite result, due to the infinite range of the Coulomb interaction. For neutrons, it yields the elastic cross section,

$$\sigma_{el} = \int d\Omega \, \frac{d\sigma}{d\Omega} = \frac{\pi}{2k^2} \sum_{lj} (2j+1) \left| 1 - S_l^j \right|^2 \, . \tag{62}$$

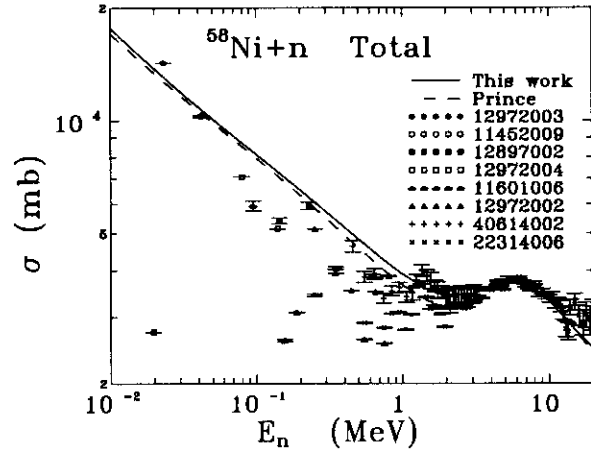This is often called the shape elastic cross section to distinguish it form the compound elastic one.

Figure 6: Various experimental measurements of the $n + ^{58} Ni$ total cross section, identified by their EXFOR access numbers, are shown together with two optical model calculations.

For neutrons, a total cross section can also be defined as the sum of the elastic and reaction cross sections,

$$\sigma_{tot} = \sigma_{el} + \sigma_r = \frac{\pi}{k^2} \sum_{lj} (2j+1)(1 - \operatorname{Re} S_l^j) \, . \tag{63}$$

The total cross section takes into account all flux lost from the incident plane wave, either by scattering or by absorption. Comparing the expression for the total cross section with that of the scattering amplitude, $A(\theta)$, one sees that the optical theorem is explicitly verified by the partial wave expansion,

$$\sigma_{tot} = \frac{4\pi}{k} \operatorname{Im} A(\theta = 0^\circ) \, . \tag{64}$$

As observed earlier, when it exists, the total optical cross section is the average of an amplitude and can thus be compared directly with the energy-averaged experimental data. This is

done in Fig. 6, where a selection of the experimental measurements of the $n +^{58} Ni$ total cross section is shown together with optical model calculations using the parameters of A. Prince[16] and those used in the exercises. Although there is a great deal of dispersion in the low energy data, the calculations succeed in following its trend.
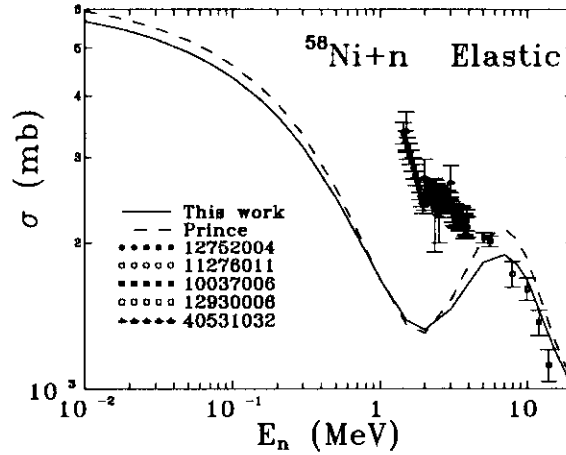

Figure 7: Various experimental measurements of the $n +^{58} Ni$ elastic cross section, identified by their EXFOR access numbers, are shown together with two optical model calculations.

The optical elastic and reaction cross sections involve the average of a squared amplitude and cannot be compared directly with the energy-averaged experimental data. The compound elastic cross section is part of the optical reaction cross section rather than the elastic cross section. The experimental elastic cross section can thus greatly exceed the optical component of the cross section. This is illustrated in Fig. 7, in which a selection of the experimental measurements of $n +^{58} Ni$ are compared to optical model calculations using the parameters of Prince[16] and of the exercises. At energies sufficiently high for the elastic compound nucleus cross section to have dropped to zero (which usually occurs at an energy of the order of a few MeV), the differential and integral (when it exists) optical elastic cross sections can be compared with the energy-averaged experimental data. Note that the elastic cross section for neutron-induced scattering can also be compared to the experimental data at extremely low incident energies, where it is customarily expressed as a scattering radius R'.

At high energies, the reaction cross section can also be compared to experimental data. However, the reaction cross section cannot be measured directly, making the data for such a comparison scarce.

6 Using ECIS95 for single-channel optical model calculations

To perform a single-channel optical model calculation with ECIS95 [17, 18, 19], one must first provide it with the parameters it needs to perform the calculation. The first of these are the system parameters — the charges and masses of the projectile and target, Z_p, A_p, Z_t, and A_t, and the relative energy, $E_{cm} = A_t E_{lab}/(A_t + A_p)$. Also needed are the parameters defining

the optical potential, the potential strengths — V, W, W_s, V_{so} and W_{so} and the geometrical parameters — the reduced radii r_i and diffusivities a_i. The spin and parity of the target ground state must also be provided, although they are actually irrelevant in the single-channel problem.

The input file to ECIS95 for a single-channel calculation is not difficult to prepare. The code, however, does not permit the input of energy-dependent parametrizations, a common characteristic of potential strengths. Instead, the strengths at each value of the energy must be calculated and entered separately. This is a task easily delegated to a small utility program. But it is then a small step to a utility program that prepares the entire input. An example of the dialogue with an interactive program of this type, PRECIS, is given in the Appendix.

Once the input is ready, the code can perform the requested calculations. This is done along the lines already discussed. For each set of system parameters, internal and external regions and a matching radius are first defined. For each partial wave, the wave function is calculated numerically in the internal region and matched to the external wave function to obtain the S-matrix element. Once the S-matrix elements are known, cross sections, transmission coefficients and angular distributions can be calculated.

ECIS95 calculates cross sections automatically. S-matrix elements (in the form $C_l^j = (S_l^j - 1)/2i$) are printed on request. Differential cross sections, polarizations and transmission coefficients are calculated and printed on request. If desired, the differential cross sections and polarizations can be plotted. However, the code does not calculate low-energy observables — the s_0 and s_1 strength functions and the scattering radius, R'.

The code ECIS95 permits comparison with and fitting to experimental data. For this, the code calculates and minimizes the χ^2, which takes the following form, for a differential cross section,

$$\chi^2 = \sum_i \left[\left(\frac{d\sigma(\theta_i)}{d\Omega} - \frac{d\sigma^x(\theta_i)}{d\Omega} \right) / \Delta\sigma^x(\theta_i) \right]^2 , \qquad (65)$$

with $d\sigma^x(\theta_i)/d\Omega$ the experimental value at angle θ_i and $\Delta\sigma^x(\theta_i)$ the experimental error. When the normalization of the experimental data is uncertain, it can also be adjusted by redefining the χ^2 as

$$\chi^2(\lambda) = \sum_i \left[\lambda \frac{d\sigma}{d\Omega}(\theta_i) - \frac{d\sigma^x}{d\Omega}(\theta_i)/\Delta\sigma^x(\theta_i) \right]^2 + [(\lambda - \lambda^x)/\Delta\lambda^x]^2 , \qquad (66)$$

where λ^x is the experimental normalization and $\Delta\lambda^x$ its error. The experimental data can be in the form of integrated and differential cross sections or polarizations. Again, the utility code PRECIS can be used to facilitate input preparation, as shown in the Appendix.

A drawback to the data fitting abilities of ECIS95 is its limitation to a single value of the relative energy at any one time. Just as it cannot utilize energy-dependent parametrizations of the potential strengths, it cannot adjust their parameters.

18

7   The generalized optical potential

The single-channel or spherical optical model treates the target nucleus as if it were spherical. But nuclei are often deformed. Even those that are spherical are often susceptible to shape oscillations. Deformed and vibrational nuclei possess low-lying collective states that are easily excited in a collision. As these excitations are prompt reaction modes, one would expect their description to lie within the scope of a generalized optical model. The standard extension of the optical model takes into account the expected deviation from spherical symmetry by modifying the radii R_i of the terms in the optical model potential.

A vibrational nucleus possesses a spherically symmetric ground state. Its excited states undergo shape oscillations about the spherical equilibrium mode.[20] To take these into account, the radii of the terms in the potential are expressed as

$$
\begin{aligned}
R_i &= R_{0i} \left(1 + \sum_{\lambda\mu} a_{\lambda\mu} Y_{\lambda\mu}(\hat{r}) \right) \\
&= R_{0i} \left(1 + \sum_{\lambda} \frac{\beta_\lambda}{\sqrt{2\lambda+1}} \sum_{\mu} (b^\dagger_{\lambda\mu} + (-)^\mu b_{\lambda-\mu}) Y_{\lambda\mu}(\hat{r}) \right) ,
\end{aligned}
\tag{67}
$$

where the $b^\dagger_{\lambda\mu}$ and $b_{\lambda\mu}$ are the creation and annihilation operators of nuclear phonons and the β_λ are the amplitudes of their respective shape oscillations. One usually expands the optical potential to first or second order in the creation and annihilation operators,

$$
\begin{aligned}
U_{opt}(r,\hat{r}) = U_{opt}(r) &+ \sum_i \frac{\partial U_{opt}}{\partial R_i} R_{0i} \sum_{\lambda\mu} a_{\lambda\mu} Y_{\lambda\mu}(\hat{r}) \\
&+ \sum_i \frac{\partial^2 U_{opt}}{\partial R_i^2} R_{0i}^2 \left(\sum_{\lambda\mu} a_{\lambda\mu} Y_{\lambda\mu}(\hat{r}) \right)^2 ,
\end{aligned}
\tag{68}
$$

thereby taking into account the direct excitation of one- and two-phonon states. The vibrational model including one-phonon states is called the first-order vibrational model, while that containing the two-photon states as well is known as the second-order model.

The nucleus ^{58}Ni serves as an example of a typical vibrational nucleus. Two neutrons from a doubly magic configuration, it has a spherically symmetric $J = 0^+$ ground state and a $J = 2^+$ excited state at E_x=1.454 MeV that can be considered a one-quadrupole-phonon vibrational state. At about twice the energy of the one-phonon state, in particular, at E_x=2.459, 2.776, and 2.943 MeV, one finds a trio of states with $J = 4^+$, 2^+, and 0^+, respectively, which can be interpreted as the two-phonon states. The fact that the first two these (but not the third) decay almost exclusively to the $J = 2^+$ excited state corroborates such an interpretation, but also shows its limitations.

A statically deformed nucleus possesses rotational excited states.[20] When the nucleus possesses axial symmetry, the radii are replaced by

$$
R_i(\theta') = R_{0i} \left(1 + \sum_\lambda \beta_\lambda Y_{\lambda 0}(\theta') \right) ,
\tag{69}
$$

19

where β_λ is the static deformation of mutipolarity λ and the angle θ' is in the body-fixed frame. This substitution could be extended to the general case of triaxial nuclei without too much difficulty (at least at this point). The model is then called the assymetric rotational model in contrast to the (axially) symmetric one. In either case, the potential obviously depends on the orientation of the principal axes of the target.

When the deformation of the nucleus is large, expansion of the potential in a Taylor series is not a good approximation. It is better to expand it directly in multipoles as

$$U_{opt}(r, \hat{r}') = \sum_\lambda U_\lambda(r) \, Y_{\lambda 0}(\hat{r}'), \tag{70}$$

where the multipole potentials are obtained as

$$U_\lambda(r) = \int d\Omega' \, U_{opt}(r, \theta') Y_{\lambda 0}(\theta') \,. \tag{71}$$

In the body-fixed frame, the moments $U_{\lambda\mu}(r)$ with $\mu \neq 0$ vanish. The body-fixed angles $\hat{r}'$ are related to the space-fixed ones $\hat{r}$ by a rotation through the angles that define the orientation of the nucleus, which are the collective angular coordinates of the nucleus, $\hat{r}_{int}$. For the spherical harmonics, this implies that

$$Y_{\lambda 0}(\hat{r}') = \sum_\mu Y_{\lambda\mu}(\hat{r}) \, D_{\mu 0}^\lambda(\hat{r}_{int}) = \sum_\mu Y_{\lambda\mu}(\hat{r}) \, Y_{\lambda\mu}^*(\hat{r}_{int}) \,, \tag{72}$$

where the $D_{\mu\mu'}^\lambda$ are rotation matrices with the special value for $\mu' = 0$ used in the last equality. The optical potential in the rotational model can thus be decomposed as

$$U_{opt}(\vec{r}, \hat{r}_{int}) = \sum_{\lambda\mu} U_\lambda(r) \, Y_{\lambda\mu}(\hat{r}) \, Y_{\lambda\mu}^*(\hat{r}_{int}) \,. \tag{73}$$

The nucleus ^{238}U provides an excellent example of a statically deformed nucleus with rotational excitations. Its 0^+ ground state possesses static quadrupolar e hexadecapolar deformations with $\beta_2 = 0.198$ and $\beta_4 = 0.057$. Its first four excited states, at $E_x - J^\pi = 0.044$ MeV-2^+, 0.148 MeV-4^+, 0.307 MeV-6^+, and 0.518 MeV-8^+, iniciate a rotational band that can be traced to at least the 28^+ state at $E_x = 4.516$ MeV. Each of these states decays exclusively to the next lower state in the rotational band.

Morel elaborate couplings between projectile and target can also be described through appropriate generalizations of the optical potential. One of these was mentioned above — the assymetric rotational model — obtained by taking into account triaxial deformations of the nucleus. Another is the vibrational-rotational model which couples static deformation to dynamic shape oscillations. More details about these can be found in Ref. 19.

The generalization of the spherical spin-orbit potential to a deformed one is not as straightforward as the above discussion would make it appear. In spin-1/2 systems, it can be obtained from the Dirac equation by eliminating the lower components of the wave function to obtain an equivalent Schrödinger equation for the upper ones. It then appears in it full Thomas form as,

$$\vec{\nabla} \, U(\vec{r}) \times -i\vec{\nabla} \cdot \vec{\sigma} \,, \tag{74}$$

20

where $\vec{\sigma}$ are the Pauli matrices. Applying this form of the coupling to a typical term in the multipole expansion, $U_\lambda(r)\,Y_{\lambda\mu}(\hat{r})$, Raynal found that its matrix element between two partial waves, $|l_i j_i\rangle$ and $|l_f j_f\rangle$, takes the form

$$
\begin{aligned}
\vec{\nabla}\left[U_\lambda(r)\,Y_{\lambda\mu}(\hat{r})\right] \times -i\vec{\nabla}\cdot\vec{\sigma} \;=\; & \langle l_f j_f|\,Y_{\lambda\mu}(\hat{r})\,|l_i j_i\rangle \left\{ \frac{1}{r}\left[\frac{d}{dr}U_\lambda(r)\right]\gamma_i \right. \\
& + \frac{U_\lambda(r)}{r}(\gamma_i-\gamma_f)\frac{d}{dr} \\
& \left. + \frac{U_\lambda(r)}{r^2}\left[\lambda(\lambda+1)-(\gamma_f-\gamma_i)(\gamma_f-\gamma_i-1)\right]\right\}\,.
\end{aligned}
$$
(75)

For the spherical optical model, $\lambda=0$, $\gamma_i=\gamma_f$ and this expression reduces to the usual one.

In the code ECIS95, six parameters z_1, z_2, z_3, z_4, z_5, and z_6 have been introduced to generalize the form of the deformed spin-orbit coupling. They appear as

$$
\begin{aligned}
\frac{1}{r}\left[\frac{d}{dr}U_\lambda(r)\right](z_1 \;+\; & z_3\gamma_i+z_4\gamma_f)+\frac{U_\lambda(r)}{r}z_6(\gamma_i-\gamma_f)\frac{d}{dr} \\
& + \; z_5\frac{U_\lambda(r)}{r^2}\left[z_2\lambda(\lambda+1)-(\gamma_f-\gamma_i)(\gamma_f-\gamma_i-1)\right]\,.
\end{aligned}
$$
(76)

The full Thomas form of the potential corresponds to the values

$$
z_1=z_4=0 \qquad\text{and}\qquad z_2=z_3=z_5=z_6=1\,.
$$
(77)

The deformed spin-orbit interaction can be increased by a factor x by using

$$
z_1=z_4=0\,, \qquad z_2=1\,, \qquad\text{and}\qquad z_3=z_5=z_6=x\,.
$$
(78)

In the generalizations of the optical potential discussed in this section, the introduction of target degrees of freedom leads to a potential that depends on the relative orientation of the target with respect to the projectile. The system is no longer invariant under independent rotations of the target or the projectile and their individual angular momenta are not conserved. However, in all cases, the system continues invariant under a simultaneous rotation of the projectile and target. The total angular momentum thus continues to be a conserved quantity.

8 Partial wave expansion in the coupled-channels optical model

The partial wave expansion proceeds in the coupled-channels optical model much as it did in the single-channel one. There are several new features however. The first of these is that the excited states and their angular momentum must now be taken into account.

To include the angular momentum of the target, the spin-angular functions are coupled to the target states to form target-spin-angular functions,

$$
\mathcal{Y}^{JM}_{lsjc}(\hat{r}) = \sum_{nN_c} \langle jnI_cN_c|JM\rangle\,\mathcal{Y}^{jn}_{ls}(\hat{r})\,|I_cN_c\rangle\,,
$$
(79)

where the $|I_cN_c\rangle$ represent the target states with total angular momentum and angular momentum projection I_c and N_c, respectively. In the vibrational model, these are the one- and

two-phonon states,

$$|I_c N_c\rangle = b^\dagger_{I_c N_c} |0\rangle \qquad \text{and} \qquad |I_c N_c\rangle = \frac{1}{\sqrt{1 + \delta_{I_1 I_2}}} \left[b^\dagger_{I_1}, b^\dagger_{I_2} \right]_{I_c N_c} |0\rangle \ . \tag{80}$$

In the axial symmetric rotational model, they are the rotational states, which can be written in terms of the rotation matrices D^I_{NK} as

$$
\begin{aligned}
\langle \vec{r}_{int} \,|I_c N_c\rangle &= \frac{1}{\sqrt{1 + \delta_{K0}}} \sqrt{\frac{2I_c + 1}{16\pi^2}} \\
&\times \left[\chi_K(\vec{r}_{int}) D^{I_c*}_{N_c K}(\hat{r}_{int}) + (-)^{I_c - I_\chi} \chi_{-K}(\vec{r}_{int}) D^{I_c*}_{N_c, -K}(\hat{r}_{int}) \right] ,
\end{aligned}
\tag{81}
$$

where $\chi_{\pm K}$ is the internal wave function of the rotational band, I_χ its internal angular momentum and K the projection of the total internal angular momentum on the symmetry axis.

The scattering wave function is expanded in a sum over both the excited states and the angular momenta. The expansion can be written as

$$\Psi = 4\pi \sum_{\substack{ljcJM \\ l'j'c'}} \mathcal{Y}^{JM}_{l'sj'c'}(\hat{r}) i^{l'} \psi^J_{l'j'c',ljc}(r) \frac{e^{i\sigma_{lc}}}{k_c r} \mathcal{Y}^{JM\dagger}_{lsjc}(\hat{k}) . \tag{82}$$

Factors of $i^{l'}$ and $e^{i\sigma_{lc}}/k_c r$, where k_c is the wave number in channel c, have again been extracted from the wave functions to simplify later manipulations. The Coulomb phase now depends on the channel energy, through k_c, as well as on the angular momentum.

In the deformed optical model, the wave functions, $\psi^J_{l'j'c',ljc}(r)$, couple different values of the angular momenta l and j and different channels c for each value of the total angular momentum J. This contrasts with the single-channel optical model, in which the wave function for total angular momentum j also possesses a well defined orbital angular momentum l. This is due to the fact that the interaction couples the different partial waves in the deformed model, while it does not do so in the spherical one. (If it did, a partial wave expansion in terms of the wave functions $\psi^j_{l'l}$ in Eq. (42) would, in general, have been necessary.)

When the partial-wave expansion of the wave function is substituted in the optical Schrödinger equation, the latter can be reduced to a set of coupled equations for each value of the total angular momentum J. These are

$$\frac{\hbar^2}{2\mu} \left\{ \frac{d^2}{dr^2} - \frac{l'(l' + 1)}{r^2} + k^2_{c'} \right\} \psi^J_{l'j'c',ljc}(r) \tag{83}$$

$$- \sum_{l''j''c''} \mathcal{U}^J_{l'j'c',l''j''c''}(r) \psi^J_{l''j''c'',ljc}(r) = 0 ,$$

where the potential matrix elements are calculated with respect to the orthonormal target-spin-angular functions,

$$\mathcal{U}^J_{l'j'c',ljc}(r) = \int d^3r_{int} \, d\Omega \, \mathcal{Y}^{JM\dagger}_{l'sj'c'}(\hat{r}) U_{opt}(\vec{r}, \vec{r}_{int}) \mathcal{Y}^{JM}_{lsjc}(\hat{r}) . \tag{84}$$

Although the target-spin-angular functions used to calculate these matrix elements have a well-defined projection M of the the total angular momentum J, the matrix elements that result are

independent of this value if the system is rotationally invariant. When the system is invariant under time-reversal, the potential matrix is also symmetric under interchange of the primed and unprimed indices.

By writing the matrix elements as matrices,

$$l'\,\delta_{l'l}\delta_{j'j}\delta_{c'c} \to L_J\,, \qquad\qquad k_{c'}\,\delta_{l'l}\delta_{j'j}\delta_{c'c} \to K_J\,, \tag{85}$$

$$\psi^J_{l'j'c',ljc}(r) \to \Psi_J(r)\,, \qquad\qquad \mathcal{U}^J_{l'j'c',ljc}(r) \to U_J(r)\,,$$

the Schrödinger equation can be recast in a more familiar form as a matrix equation,

$$\left\{ \frac{d^2}{dr^2} - \frac{L_J(L_J+1)}{r^2} + K_J^2 - \frac{2\mu}{\hbar^2} U_J(r) \right\} \Psi_J(r) = 0\,. \tag{86}$$

The incoming-wave boundary condition again requires that asymptotically the wave function take the form of an incoming plane wave and an outgoing scattering wave. Here this takes the form

$$\Psi \to \sum_c \exp\left(i\vec{k}_c \cdot \vec{r} + i\eta_c \log(k_c r \quad - \quad \vec{k}_c \cdot \vec{r}) \right) \sum_\nu |s\nu I_c N_c\rangle \langle s\nu I_c N_c|$$

$$+ \frac{1}{r} \sum_{cc'} \exp\left(i k_{c'} r \quad - \quad i\eta_{c'} \log(2k_{c'} r) \right) \tag{87}$$

$$\times \sum_{\nu\nu'} |s\nu' I_{c'} N_{c'}\rangle \overline{f}_{\nu' N_{c'} \nu N_c}(\theta) \langle s\nu I_c N_c|\,,$$

where the $\overline{f}_{\nu' N_{c'} \nu N_c}(\theta)$ are the target and projectile spin-projected matrix elements of the elastic scattering amplitude.

The asymptotic form expected of the wave function in the partial wave of total angular momentum J can be most easily expressed using an obvious extension of the matrix notation above. To be consistent with Eq. (87) and satisfy the differential equation, the matrix wave function Ψ_J must have for its asymptotic form,

$$\Psi_J(r) \to F_J(r) \quad + \quad (G_J(r) + iF_J(r))\,\overline{C}_J \tag{88}$$

$$= \frac{i}{2}\left(H_J^-(r) - H_J^+(r)e^{i\sigma_J}\overline{S}_J e^{i\sigma_J} \right) e^{-i\sigma_J}\,,$$

where $\overline{C}_J = (\overline{S}_J - 1_J)/2i$, F_J and G_J are the regular and irregular Coulomb wave functions in (diagonal) matrix form, respectively, and $H_J^\pm = e^{\mp i\sigma_J}(G_J \pm iF_J)$ are the linear combinations of these that asymptotically contain only incoming (H_J^-) or outgoing (H_J^+) waves. $\overline{S}_J$ is the nuclear part of the S-matrix element. One can loosely interpret the half of the Coulomb phase shift $e^{i\sigma_J}$ that precedes the nuclear S-matrix in Eq. (88) as the Coulomb deflection accumulated on the incoming half of the 'trajectory,' with the half of the Coulomb phase shift following the nuclear S-matrix then being the Coulomb deflection of the outgoing half of the 'trajectory'.

The S-matrix elements, S_J, can be obtained by an obvious extension of the method used for the spherical optical model. In the internal region, the differential equation for each partial wave, Eq. (86) is solved numerically out to the radius, r_m. The numerical solution and its derivative

23

are matched there to the wave function in the external region, given by Eq. (88), and to its derivative, to obtain the amplitudes in the internal region, a_J, and the S-matrix elements, S_J. This is repeated for increasing values of J until the value of S_J which results is sufficiently close to one.

The important difference between the deformed optical model and the spherical model is that the wave function in partial wave J is not a scalar, as it is in the spherical model, but a matrix. The differential equation that must be solved is also a matrix one. Although the only solution that is normally of interest is the one in which the target is in its ground state in the incoming wave, the complete matrix solution is needed to invert the matching equations and obtain the S-matrix. The calculation is thus much more time consuming than in the spherical case.

To obtain the partial wave expansion of the scattering amplitude, one repeats the procedure used earlier: substitute the asymptotic form of the partial wave function, Ψ_J of Eq. (88), in the partial wave expansion of the total wave function, Eq. (82), and compare the result to the expected form of the asymptotic wave function, Eq. (87). One then finds

$$\overline{f}(\theta) = \frac{4\pi}{2i} \sum_{\substack{ljcJM \\ l'j'c'}} \left(e^{i\sigma_{l'c'}} \overline{S}^J_{l'j'c',ljc} e^{i\sigma_{lc}} - \delta_{l'l}\delta_{j'j}\delta_{c'c} \right) \frac{1}{k_c} \mathcal{Y}^{JN}_{l'sj'c'}(\hat{r}) \mathcal{Y}^{JN\dagger}_{lsjc}(\hat{k}) . \tag{89}$$

Its target and projectile spin-projected matrix elements are

$$\begin{aligned}
\overline{f}_{\nu'N_{c'}\nu N_c}(\theta) &= \frac{4\pi}{2i} \sum_{\substack{ljcl'j'c' \\ JMmm'nn'}} \left(e^{i\sigma_{l'c'}} \overline{S}^J_{l'j'c',ljc} e^{i\sigma_{lc}} - \delta_{l'l}\delta_{j'j}\delta_{c'c} \right) \frac{1}{k_c} \\
&\quad \times Y_{l'm'}(\hat{r}) Y^*_{lm}(\hat{k}) \langle l'm's\nu'|j'n' \rangle \tag{90} \\
&\quad \times \langle j'n'I_{c'}N_{c'}|JM \rangle \langle JM|jnI_cN_c \rangle \langle jn|lms\nu \rangle .
\end{aligned}$$

In the scattering problem considered here, the flux, not the density, is conserved. When a state is excited, the energy that goes to excitation must be taken from the relative motion. The relative velocity thus decreases, as does the flux. To take this into account, the S-matrix and scattering amplitude must be renormalized as

$$S^J_{l'j'c',ljc} = \sqrt{\frac{k_{c'}}{k_c}} \, \overline{S}^J_{l'j'c'ljc} \qquad \text{or} \qquad S_J = K_J^{1/2} \, \overline{S}_J \, K_J^{-1/2} , \tag{91}$$

and

$$f_{\nu'N_{c'}\nu N_c}(\theta) = \sqrt{\frac{k_{c'}}{k_c}} \, \overline{f}_{\nu'N_{c'}\nu N_c}(\theta) . \tag{92}$$

When the system is time-reversal invariant, the matrix S_J is symmetric.

The scattering amplitude with the Coulomb term extracted thus has the form

$$\begin{aligned}
f_{\nu'N_{c'}\nu N_c}(\theta) &= \delta_{\nu'\nu}\delta_{N_{c'}N_c} f_{Cc}(\theta) \\
&\quad + \frac{4\pi}{2i} \sum_{\substack{ljcl'j'c' \\ JMmm'nn'}} e^{i\sigma_{l'c'}} \left(S^J_{l'j'c',ljc} - \delta_{l'l}\delta_{j'j}\delta_{c'c} \right) e^{i\sigma_{lc}} \frac{1}{k_c} \\
&\quad \times Y_{l'm'}(\hat{r}) Y^*_{lm}(\hat{k}) \langle l'm's\nu'|j'n' \rangle \tag{93} \\
&\quad \times \langle j'n'I_{c'}N_{c'}|JM \rangle \langle JM|jnI_cN_c \rangle \langle jn|lms\nu \rangle .
\end{aligned}$$

24

where

$$f_{Cc}(\theta) = -\frac{\eta_c}{2k_c \sin^2 \theta/2} \exp\left[-i\eta_c \log\left(\sin^2 \theta/2\right) + 2i\sigma_{0c}\right] \tag{94}$$

is the Coulomb amplitude in channel c.

Once the scattering amplitude is known, calculating cross sections is a simple matter. The differential cross sections for an unpolarized incident beam and target are obtained by averaging the squared magnitude of the scattering amplitudes over the initial values of the projectile and target spin and summing over the final values. The differential elastic cross section for a collision in which the target is initially in its ground state is then given by

$$\frac{d\sigma_{el}}{d\Omega} = \frac{1}{(2s+1)(2I_0+1)} \sum_{\substack{\nu' N_0' \\ \nu N_0}} \left| f_{\nu' N_0' \nu N_0}(\theta) \right|^2 . \tag{95}$$

The differential inelastic cross section for inelastic scattering to an excited state c can be written similarly as

$$\frac{d\sigma_c}{d\Omega} = \frac{1}{(2s+1)(2I_0+1)} \sum_{\substack{\nu' N_c' \\ \nu N_0}} \left| f_{\nu' N_c' \nu N_0}(\theta) \right|^2 , \tag{96}$$

where it should be emphasized that the sum over N_c' refers to a sum over the spin projections of the final state c only.

Due to the infinite range of the Coulomb force, the integrated elastic cross section is finite only when at least one of the two colliding particles is neutral. In the particular case of neutrons incident on a nucleus, integration of the differential cross section of Eq. (95) yields.

$$\sigma_{el} = \frac{1}{2(2I_0+1)} \frac{\pi}{k^2} \sum_{\substack{l'j'lj \\ J}} (2J+1) \left| S^J_{l'j'c_0,ljc_0} - \delta_{l'l}\delta_{j'j} \right|^2 . \tag{97}$$

The integrated inelastic cross sections exist for for both neutral and charged particles. They take the form

$$\sigma_c = \frac{1}{(2s+1)(2I_0+1)} \frac{\pi}{k^2} \sum_{\substack{l'j'lj \\ J}} (2J+1) \left| S^J_{l'j'c,ljc_0} \right|^2 \qquad c \neq c_0 . \tag{98}$$

Just as in the single-channel problem, the total flux lost from the elastic channel can be related to the reaction cross section through the equation

$$\sigma_r = -\frac{1}{v} \oint \vec{j}_0 \cdot d\vec{a} , \tag{99}$$

where the probability current,

$$\vec{j}_0 = \frac{\hbar}{2i\mu} \left(\Psi_0^\dagger \nabla \Psi_0 - (\nabla \Psi_0)^\dagger \Psi_0 \right) , \tag{100}$$

is integrated over a surface which tends to infinity, with Ψ_0 being the ground-state component of the wave function. However, in the coupled-channel problem, it is also possible to define an

25

absorption cross section, which can be related to the total flux lost from all channels, elastic and inelastic, as

$$\sigma_{abs} = -\frac{1}{v} \oint \sum_c \vec{j_c} \cdot d\vec{a}, \tag{101}$$

where the probability current in channel c, $\vec{j_c}$, is

$$\vec{j_c} = \frac{\hbar}{2i\mu} \left(\Psi_c^\dagger \nabla \Psi_c - (\nabla \Psi_c)^\dagger \Psi_c \right), \tag{102}$$

with Ψ_c the component of the wave function that asymptotically occupies state c.

Using the asymptotic form of the partial waves, Eq. (88), the expression for the reaction cross section can be reduced to

$$\sigma_r = \frac{1}{(2s+1)(2I_0+1)} \frac{\pi}{k^2} \sum_{\substack{l'j'lj \\ cJ}} (2J+1) \left(\delta_{l'l}\delta_{j'j} - \left| S^J_{l'j'c_0,ljc_0} \right|^2 \right). \tag{103}$$

The contribution of each partial wave to the reaction cross section is determined by the fraction of the flux lost from the elastic channel. The absorption cross section can, of course, be reduced to a similiar form, which can be written as

$$\sigma_{abs} = \frac{1}{(2s+1)(2I_0+1)} \frac{\pi}{k^2} \sum_{ljJ} (2J+1) \, T^J_{ljc_0,ljc_0}, \tag{104}$$

where the coupled-channels transmission coefficients have been introduced. These are defined as

$$T^J_{l'j'c',ljc} = \delta_{l'l}\delta_{j'j}\delta_{c'c} - \sum_{l''j''c''} S^{J*}_{l''j''c'',l'j'c'} S^J_{l''j''c'',ljc}. \tag{105}$$

The similarity of the transmission coefficients to the single-channel ones becomes clear when they are written in matrix form. The transmission matrix in partial wave J can be written in terms of the corresponding S-matrix as

$$T_J = 1_J - S_J^\dagger S_J. \tag{106}$$

Comparison of the form of the reaction and absorption cross sections reveals a simple relation between the two,

$$\sigma_r = \sigma_{abs} + \sum_{c \neq c_0} \sigma_c. \tag{107}$$

In other words, the elastic channel loses flux to both the prompt inelastic channels and the long-lived compound states. The reaction cross section takes both of these into account.

The absorption cross section and the corresponding transmission coefficients characterize the transition of flux from the prompt channels to the compound states. These are the quantities of principal interest for compound-nucleus calculations. When using coupled-channels transmission coefficients in compound-nucleus calculations, it is quite common to use just the diagonal elements of the transmission matrix and neglect the off-diagonal ones. A careful analysis by

Engelbrecht and Weidenmüller [22] showed that a more correct procedure is to perform the compound-nucleus calculation in a basis in which the transmission coefficients are diagonal and transform the resulting cross sections back to the non-diagonal basis. ECIS95 can, in fact, perform such an analysis. However, discussion of this feature of the code requires entering fairly deeply into the details of the statistical model, which will not be done here.

For neutral particles, the neutron in particular, the elastic cross section is finite. A total cross section can then be defined as the sum of the elastic and reaction cross sections,

$$\sigma_{tot} = \sigma_{el} + \sigma_r = \frac{1}{2I_0 + 1} \frac{\pi}{k^2} \sum_{ljJ} (2J + 1)(1 - \text{Re}\, S^J_{ljc_0,ljc_0}) \,. \tag{108}$$

The total cross section takes into account the occurence of scattering of any type. It is a measure of the flux lost from the incident plane wave state.
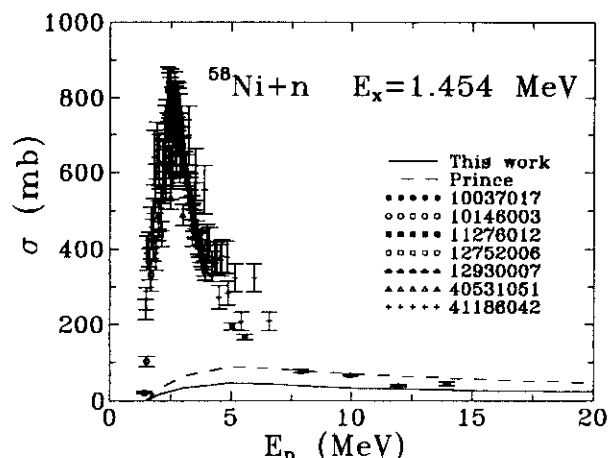

Figure 8: Various experimental measurements of the $n +^{58} Ni$ $E_x=1.454$ MeV 2^+ inelastic cross section, identified by their EXFOR access numbers, are shown together with two optical model calculations.

Just as in the case of the elastic cross section, care must be taken when comparing inelastic optical model cross sections with experimental data. At low energies, these cross sections are dominated by their compound nucleus contribution, as shown in Figs. 8 and 9, for neutron-induced excitation of the first excited state in ^{58}Ni and ^{238}U, respectively. One observes that the direct process plays a very minor role in the excitation of these states in the first few MeV above threshhold. In Fig. 8, the ^{58}Ni data are compared to optical model calculations using the parameters of A. Prince[16] and those of the exercises, both with a phonon amplitude of $\beta_2=0.2$. Note the strong influence of the optical model parameters on the direct component of the inelastic ^{58}Ni excitation. The Prince parameters yield an inelastic cross section that is almost twice that of the parameters of the exercises, although both use the same phonon amplitude. The ^{238}U data of Fig. 9 is compared to an optical model calculation using the parameters of Young and Arthur[21], which fits the higher energy data quite well. One notes that the direct excitation cross section of the ^{238}U 2^+ state reaches a value of almost 500 mb. In general, the inelastic

excitation of a rotational band can be quite large, demanding a coupled channels method for its precise calculation.
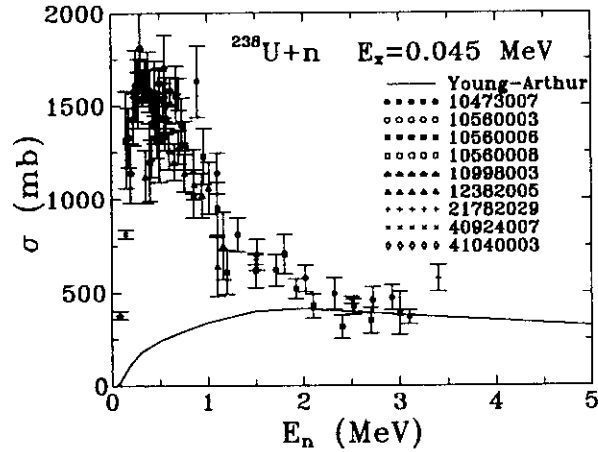

Figure 9: Various experimental measurements of the $n +^{238} U$ E_x=0.044 MeV 2^+ inelastic cross section, identified by their EXFOR access numbers, are shown together with an optical model calculation.

9 Using ECIS95 for coupled-channels optical model calculations

Most of the information needed to perform a coupled-channels optical model calculation using ECIS95 is already needed to perform the single-channel calculation. This information consists of the system parameters — the charges and masses of the projectile and target, Z_p, A_p, Z_t, and A_t, and the relative energy, E_{cm}, as well as the potential strengths — V, W, W_s, V_{so} and W_{so} and the geometrical parameters — the reduced radii r_i and diffusivities a_i.

The additional information that must be furnished concerns the excited states of the target and the oscillation amplitudes or deformation parameters that determine their excitation. The excitation energy, spin and parity of each of the excited states must be provided to the code. The spin and parity of the ground state, requested but irrelevant to the single channel case, are also necessary now. (Although only the total angular momentum has been mentioned, parity is also conserved in purely nuclear reactions.)

In the vibrational model, an excited state can be a one-phonon state, a two phonon state or a mixture of the two. ECIS95 requires this information to calculate the coupling correctly. When a state is a mixture of one- and two-phonon states, the code also requires a mixing parameter. In the pure symmetric rotational model, all possible excited states are members of the same rotational band and more information on their structure is unnecessary.

In the vibrational model, each phonon must be characterized by its angular momentum and amplitude of oscillation. In the rotational model, the static deformations ($\lambda = 2, 4, ...$) must be furnished. In this case, one must also furnish the maximum value of λ to be used in the multipole expansion of the potential. A reasonable value for this parameter is twice the angular

momentum of the most highly excited state. Terms in the multipole expansion with λ larger than this value have no effect and need not be included. The exclusion of terms with λ smaller than this value omits coupling and reorientation terms that are usually small but that can still have observable effects.

The simplest description of the phonon amplitudes or the static deformations assumes them to be the same for all deformed terms in the optical potential. It is also possible to use a different set of phonon amplitudes or deformations for each term in the potential. In fact, it is even possible to furnish a different set of optical model parameters for each of the states. In this case, it is the ground state potential that is deformed to obtain the coupling matrix elements.

With the input prepared, the code performs the calculations along the lines discussed earlier. It calculates cross sections automatically while S-matrix elements (in the form $C_l^j = (S_l^j - 1)/2i$) are printed on request. Differential cross sections, polarizations and transmission coefficients are also calculated and printed on request. If desired, the differential cross sections and polarizations can be plotted. The code permits comparison with and fitting to experimental data, as in the single-channel case, with the same restriction to a single value of the relative energy. An interesting feature that is particular to the coupled-channels case is the ability to adjust the sum of cross sections for two or more states to unresolved experimental cross sections.

10   The ECIS method

The ECIS method (Equations Couplées en Itérations Séquentielles — Sequential iteration of coupled equations) provides an alternative to the conventional matrix method of performing coupled-channels calculations. Instead of the differential representation of the wave equation, the Schrödinger equation, it uses its integral representation, the Lippmann-Schwinger equation,

$$\Psi = \Psi_0^+ + G_0^+ U' \Psi , \tag{109}$$

where G_0^+ is the Green's function of the same Schrödinger equation satisfied by Ψ_0^+ and the $+$ superscript means that the wave function Ψ_0^+ satisfies incoming-wave bounday conditions while the propagator G_0^+ asymptotically contains only outgoing waves. The ECIS method takes advantage of the structure of the Lippmann-Schwinger equation by placing the diagonal solution of the single-channel optical model in Ψ_0^+ and G_0^+ and relegating the channel coupling to the interaction term, U'.

In the single-channel optical model problem, one can define incoming- and outgoing-wave solutions, $h_{lc}^{j\pm}(r)$, of the wave equation in each channel,

$$\left\{ \frac{d^2}{dr^2} - \frac{l(l+1)}{r^2} + k_c^2 - \frac{2\mu}{\hbar^2} \left(U_{cen,c}(r) + d_l^j U_{so,c}(r) \right) \right\} h_{lc}^{j\pm}(r) = 0 , \tag{110}$$

where the spin-orbit constant $d_l^j = d_{so} \left(j(j+1) - l(l+1) - s(s+1) \right)/2$ is as before. Asymptotically, these solutions have the same behavior as the incoming and outgoing Coulomb waves,

$$h_{lc}^{j\pm}(r) \to H_{lc}^\pm(r) = e^{\mp i\sigma_{lc}} \left(G_{lc}(r) \pm i F_{lc}(r) \right) . \tag{111}$$

They are, however, solutions to the optical Schrödinger equation at all values of r. Numerically, they can be obtained by solving the differential equation inward from the matching point, using the conditions for matching to the asymptotic Coulomb functions as the initial conditions.

The incoming- and outgoing- wave solutions to the optical Schrödinger equation are not regular at the origin. Through a comparison with the asymptotic form given in Eq. (46), it is easy to convince oneself that a linear combination of the two that is regular is given in terms of the S-matrix as

$$
\begin{aligned}
\psi_{lc}^{j+}(r) &= \frac{i}{2}\left(h_{lc}^{j-}(r) - h_{lc}^{j+}(r)e^{2i\sigma_{lc}}S_{0lc}^{j}\right) \\
&= \psi_{lc}^{j}(r)e^{i\sigma_{lc}},
\end{aligned} \tag{112}
$$

where the last equality simply makes note of the relationship between the wave function ψ_{lc}^{j+} and the single-channel wave function ψ_{lc}^{j} of the partial wave expansion in Eq. (42). The S-matrix has been relabelled S_0 to emphasize its relation to the single-channel problem as well.

The single-channel Green's function in channel c can be decomposed in partial waves as

$$
G_{0c}^{+}(\vec{r},\vec{r}') = \frac{1}{rr'}\sum_{ljn}\mathcal{Y}_{ls}^{jn}(\hat{r})\, g_{lc}^{j+}(r,r')\mathcal{Y}_{ls}^{jn\dagger}(\hat{r}'), \cdot \tag{113}
$$

where the partial-wave Green's functions are defined in terms of the regular and outgoing partial wave solutions as

$$
g_{lc}^{j+}(r,r') = -\frac{2\mu}{\hbar^{2}k_{c}}\psi_{lc}^{j+}(r_{<})\, h_{lc}^{j+}(r_{>}). \tag{114}
$$

The channel Green's functions can then be combined into the complete single-channel Green's function appropriate to the coupled-channels problem,

$$
\begin{aligned}
G_{0}^{+}(\vec{r},\vec{r}') &= \sum_{cN_c} G_{0c}^{+}(\vec{r},\vec{r}')\,|I_cN_c\rangle\langle I_cN_c| \tag{115} \\
&= \frac{1}{rr'}\sum_{\substack{ljc \\ JM}}\mathcal{Y}_{lsj}^{JM}(\hat{r})\, g_{lc}^{j+}(r,r')\,\mathcal{Y}_{lsj}^{JM\dagger}(\hat{r}').
\end{aligned}
$$

When the partial wave expansions, Eqs. (82) and (115), are substituted in the Lippmann-Schwinger equation, Eq. (109), it can be reduced to a set of coupled equations for each partial wave,

$$
\begin{aligned}
\psi_{l'j'c',ljc}^{J}(r) &= \psi_{lc}^{j}(r)\delta_{l'l}\delta_{j'j}\delta_{c'c} \tag{116} \\
&+ \int_{0}^{\infty} dr'\, g_{l'c'}^{j'+}(r,r') \sum_{l''j''c''}\mathcal{U}_{l'j'c',l''j''c''}^{lJ}(r')\psi_{l''j''c'',ljc}^{J}(r').
\end{aligned}
$$

In matrix notation, this takes a much simpler form,

$$
\Psi_J(r) = \Psi_{0J}(r) + \int_{0}^{\infty} dr'\, G_{0J}^{+}(r,r')\, U_J'(r')\,\Psi_J(r'), \tag{117}
$$

30

where $\Psi_{0J} = \Psi_{0J}^+ e^{i\sigma_J}$ is the coupled-channels (diagonal) matrix form of the single-channel wave function of Eq. (42). Asymptotically, this partial wave equation tends to

$$\frac{i}{2}\left(H_J^-(r) \quad - \quad H_J^+(r)e^{i\sigma_J}\overline{S}_J e^{i\sigma_J}\right)e^{-i\sigma_J}$$

$$= \quad \frac{i}{2}\left(H_J^-(r) - H_J^+(r)e^{i\sigma_J}S_{0J}e^{i\sigma_J}\right)e^{-i\sigma_J} \tag{118}$$

$$-H_J^+(r)\frac{2\mu}{\hbar^2}K_J^{-1}e^{i\sigma_J}\int_0^\infty dr'\Psi_{0J}(r')\,U_J'(r')\,\Psi_J(r')\,.$$

Extracting the coefficient of the outgoing Coulomb wave, H_J^+, one obtains an expression for the coupled-channels S-matrix,

$$S_J = S_{0J} + 2i\frac{2\mu}{\hbar^2}K_J^{-1/2}\int_0^\infty dr'\,\Psi_{0J}(r')\,U_J'(r')\,\Psi_J(r')\,K_J^{-1/2}\,. \tag{119}$$

(Recall that $S_J = K_J^{1/2}\,\overline{S}_J\,K_J^{-1/2}$.)

The drawback to this form of obtaining the S-matrix is that it first requires knowledge of the full coupled-channels wave function. The ECIS method tries to obtain this knowledge by solving the partial-wave Lippmann-Schwinger equation, Eq. (117), iteratively. To describe the method precisely and simply, the notation in use must be modified slightly to permit a compact representation of the submatrices between two channels in a given partial wave, an example being the component of the interaction, $\mathcal{U}_{c'c}'$, where the partial wave index J has been suppressed. The matrix structure of $\mathcal{U}_{c'c}'$ takes into account the $l'j', lj$ dependence.

The ECIS method first assumes that the excited states have been arranged in order of decreasing coupling with the ground state. It begins iterating by using the single-channel ground-state wave function as the zeroth-order approximation to the coupled-channels ground-state wave function, $\Psi_0^{(0)}(r) = \Psi_{0c_0}(r)$.

The first-order approximation to the wave function of the first excited state is

$$\Psi_1^{(1)}(r) = \int_0^\infty dr'\,g_1^+(r,r')\mathcal{U}_{10}'(r')\,\Psi_0^{(0)}(r')\,, \tag{120}$$

with the corresponding approximation to its S-matrix element being

$$S_1^{(1)} = 2i\frac{2\mu}{\hbar^2\sqrt{k_0 k_1}}\int_0^\infty dr'\,\Psi_{0c_1}(r')\mathcal{U}_{10}'(r')\,\Psi_0^{(0)}(r')\,. \tag{121}$$

The first-order iteration to the wave function of excited state j is given by

$$\Psi_j^{(1)}(r) = \int_0^\infty dr'\,g_j^+(r,r')\left[\mathcal{U}_{j0}'(r')\,\Psi_0^{(0)}(r') + \sum_{i=1}^{j-1}\mathcal{U}_{ji}'(r')\,\Psi_i^{(1)}(r')\right]\,, \tag{122}$$

with the approximation to the S-matrix element being

$$S_j^{(1)} \quad = \quad 2i\frac{2\mu}{\hbar^2\sqrt{k_0 k_j}}\int_0^\infty dr'\,\Psi_{0c_j}(r')\,[\,\mathcal{U}_{j0}'(r')\,\Psi_0^{(0)}(r') \tag{123}$$

$$+ \sum_{i=1}^{j-1}\mathcal{U}_{ji}'(r')\,\Psi_i^{(1)}(r')\,]\,.$$

Note that the jth excited-state wave function is not given merely in terms of the zeroth-order approximation to the wave function, which contributes the first term in the expressions above. It also makes use of the $j - 1$ first-order wave functions already calculated to improve the approximation.

After approximating each of the N excited states in turn, the first-order iteration is concluded at step $N + 1$ by correcting the ground-state wave function,

$$\Psi_0^{(1)}(r) = \Psi_{0c_0}(r) + \int_0^\infty dr' \, g_0^+(r,r') \, [\, \mathcal{U}_{00}'(r') \, \Psi_0^{(0)}(r') \tag{124}$$
$$+ \sum_{i=1}^N \mathcal{U}_{0i}'(r') \, \Psi_i^{(1)}(r') \,] \,,$$

and S-matrix element,

$$S_0^{(1)} = S_{0c_0} + 2i \frac{2\mu}{\hbar^2 k_0} \int_0^\infty dr' \, \Psi_{0c_0}(r') \, [\, \mathcal{U}_{00}'(r') \, \Psi_0^{(0)}(r') \tag{125}$$
$$+ \sum_{i=1}^N \mathcal{U}_{0i}'(r') \, \Psi_i^{(1)}(r') \,] \,,$$

where S_{0c_0} is the single-channel ground-state S-matrix element.

In the successive iterations, the most recent approximation to the wave function in each of the channels is used. In iteration m, for example, each of the N excited states are approximated as

$$\Psi_j^{(m)}(r) = \int_0^\infty dr' \, g_j^+(r,r') \, [\, \sum_{i=j}^N \mathcal{U}_{ji}'(r') \, \Psi_i^{(m-1)}(r') \tag{126}$$
$$+ \mathcal{U}_{j0}'(r') \, \Psi_0^{(m-1)}(r') + \sum_{i=1}^{j-1} \mathcal{U}_{ji}'(r') \, \Psi_i^{(m)}(r') \,] \,,$$

with corresponding S-matrix elements

$$S_j^{(m)} = 2i \frac{2\mu}{\hbar^2 \sqrt{k_0 k_j}} \int_0^\infty dr' \, \Psi_{0c_j}(r') \, [\, \sum_{i=j}^N \mathcal{U}_{ji}'(r') \, \Psi_i^{(m-1)}(r') \tag{127}$$
$$+ \mathcal{U}_{j0}'(r') \, \Psi_0^{(m-1)}(r') + \sum_{i=1}^{j-1} \mathcal{U}_{ji}'(r') \, \Psi_i^{(m)}(r') \,] \,.$$

The iteration concludes with a new approximation to the ground-state wave function

$$\Psi_0^{(m)}(r) = \Psi_{0c_0}(r) + \int_0^\infty dr' \, g_0^+(r,r') \, [\, \mathcal{U}_{00}'(r') \, \Psi_0^{(m-1)}(r') \tag{128}$$
$$+ \sum_{i=1}^N \mathcal{U}_{0i}'(r') \, \Psi_i^{(m)}(r') \,] \,,$$

and S-matrix element,

$$S_0^{(m)} = S_{0c_0} + 2i \frac{2\mu}{\hbar^2 k_0} \int_0^\infty dr' \, \Psi_{0c_0}(r') \, [\, \mathcal{U}_{00}'(r') \, \Psi_0^{(m-1)}(r') \tag{129}$$
$$+ \sum_{i=1}^N \mathcal{U}_{0i}'(r') \, \Psi_i^{(m)}(r') \,] \,.$$

Iteration of the equations is continued until the S-matrix converges. Unfortunately, this does not always occur when the coupling is strong. The code ECIS95 can attempt to improve the convergence through the use of Padé approximants. These attempt to approximate a power series expansion in terms of a ratio of polynomials. To this end, ECIS95 actually solves the Lippmann-Schwinger equation in the form

$$\Psi = \Psi_0^+ + \lambda\, G_0^+\, U'\, \Psi\,, \tag{130}$$

where λ is a multiplicative factor that is taken to be one at the end of the calculation. In practice, this is done by storing the intermediate results for each state independently at each iteration.

The ECIS method has two advantages over the usual method of solving the coupled-channels problem. The first and most important is that it need only solve the system of equations with the incoming-wave boundary condition of physical interest. The conventional method requires solutions for all possible incoming waves, in order to invert the matching equations and obtain the S-matrix. Thus, even though the ECIS method is iterative, it is often much faster than the conventional method of solution.

A second advantage of the ECIS method is that it permits calculations using deformed spin-orbit potentials. The integration method used by ECIS95 to numerically solve the differential equations takes advantage of the standard form of the radial Schrödinger equation, which contains second derivatives but no first derivatives. As the deformed spin-orbit potential of Eq. (75) normally contains first derivatives, it would require another method of integration. The alternative is to use the ECIS method, which has no restrictions of this type.

11 The distorted-wave Born approximation

The distorted-wave Born approximations (DWBA) can be understood as a simple iterative expansion of the Lippmann-Schwinger equation in powers of the potential. It is thus a good approximation when the coupling is weak.

Making use of the general expressions for a partial wave J, Eqs. (117) and (119), one has for the zeroth-order approximations (starting values) for the wave function and S-matrix,

$$\Psi_J^{(0)}(r) = \Psi_{0J}(r) \qquad \text{and} \qquad S_J^{(1)} = S_{0J}\,. \tag{131}$$

The first-order distorted-wave Born approximation, or just DWBA, to the wave function is then

$$\Psi_J^{(1)}(r) = \Psi_{0J}(r) + \int_0^\infty dr'\, G_{0J}^+(r,r')\, U_J'(r')\, \Psi_{0J}(r')\,, \tag{132}$$

while the DWBA to the S-matrix is

$$S_J^{(1)} = S_{0J} + 2i\frac{2\mu}{\hbar^2}\, K_J^{-1/2} \int_0^\infty dr'\, \Psi_{0J}(r')\, U_J'(r')\, \Psi_{0J}(r')\, K_J^{-1/2}\,. \tag{133}$$

Note that the S-matrix is clearly symmetric when the optical potential matrix U_J' is symmetric.

The DWBA is at times extended to second order in the coupling. In this case, one obtains for the wave function,

$$
\Psi_J^{(2)}(r) = \Psi_{0J}(r) + \int_0^\infty dr'\, G_{0J}^+(r,r')\, U_J'(r')\, \Psi_{0J}(r') \tag{134}
$$
$$
+ \int_0^\infty dr'\, G_{0J}^+(r,r')\, U_J'(r') \int_0^\infty dr''\, G_{0J}^+(r',r'')\, U_J'(r'')\, \Psi_{0J}(r'')\,,
$$

and for the S-matrix

$$
S_J^{(2)} = S_{0J} + 2i\frac{2\mu}{\hbar^2} K_J^{-1/2} \int_0^\infty dr'\, \Psi_{0J}(r')\, U_J'(r')\, \Psi_{0J}(r')\, K_J^{-1/2}
$$
$$
+ 2i\frac{2\mu}{\hbar^2} K_J^{-1/2} \int_0^\infty dr'\, \Psi_{0J}(r')\, U_J'(r') \tag{135}
$$
$$
\times \int_0^\infty dr''\, G_{0J}^+(r',r'')\, U_J'(r'')\, \Psi_{0J}(r'')\, K_J^{-1/2}\,.
$$

The DWBA is usually not extended beyond second order. If higher order terms in the interaction are necessary, it is usually better to resort to other methods, such as the conventional or ECIS methods for coupled-channels calculations.

Although similar in form, the ECIS method and the DWBA are not equivalent. The first-order DWBA contains terms of at most first order in the coupling. In the ECIS method, this is necessarily the case only for the first excited state in the first iteration. The approximation to the second state, in the first iteration of the ECIS method, contains a second-order contribution obtained by coupling the ground state to the first excited state and the latter to the second excited state. This term appears in the DWBA only in the second-order approximation.

The DWBA was developed to approximate the effects of the coupling between channels when that coupling is weak. It assumes that the contribution of the next-order term will always be relatively small compared to the last term included, due to the weakness of the coupling. The goal of the ECIS method is to solve the coupled-channels problem quickly and efficiently, irregardless of the magnitude of the coupling. It thus makes use of all the information it has on hand.

12   Reduced matrix elements and form factors

In Eq. (84), the target-spin-angular functions were used to calculate the matrix elements of the optical potential,

$$
\mathcal{U}_{l'j'c',ljc}^J(r) = \int d^3r_{int}\, d\Omega\, \mathcal{Y}_{l'sj'c'}^{JM\dagger}(\hat{r})\, U_{opt}(\vec{r},\vec{r}_{int})\, \mathcal{Y}_{lsjc}^{JM}(\hat{r})\,. \tag{136}
$$

It was noted that although these elements are calculated for a particular value M of the projection of the total angular momentum J, the matrix elements that result are independent of this value if the system is rotationally invariant. The representation of these matrix elements will be discussed here.

The most general form of a rotationally-invariant interaction between a projectile and a target couples tensor operators acting on the orbital angular momentum, $i^\lambda Y_{\lambda\mu}(\hat{r})$, the spin of

34

the projectile, $Q^p_{\sigma\nu}$, and the angular momentum of the target, $Q^t_{\kappa\xi}(\vec{r}_{int})$, to a scalar,

$$U_{opt}(\vec{r},\vec{r}_{int}) = \sum_{\lambda\sigma\kappa} V^{c'c}_{\lambda\sigma\kappa}(r)\, i^\lambda\, Y_{\lambda\mu}(\hat{r})\, Q^p_{\sigma\nu}\, Q^t_{\kappa\xi}(\vec{r}_{int}) \begin{pmatrix} \lambda & \sigma & \kappa \\ \mu & \nu & \xi \end{pmatrix} . \tag{137}$$

In principle, the radial dependence of each term, $V^{c'c}_{\lambda\sigma\kappa}(r)$, can depend on the angular momenta of the tensor operators, λ, σ, and κ, as well as on the initial and final channels, c and c'.

The interactions in the vibrational and rotational models (with a spherical spin-orbit potential) are simpler than the general one above, as they couple only the orbital and target angular momenta. In these cases, the projectile-spin tensor operator is itself a scalar. This is not true in general, as can be seen from the form of the deformed spin-orbit potential in Eq. (75).

The matrix elements of the general interaction of Eq. (137), calculated with respect to the target-spin-angular functions, can always be written in the form

$$\mathcal{U}^J_{l's'j'c',lsjc}(r) = \frac{1}{\sqrt{4\pi}} \sum_{\lambda\sigma\kappa} G^{J\lambda\sigma\kappa}_{l's'j'c',lsjc} \langle s'|\,Q^p_\sigma\,|s\rangle \langle I_{c'}|\,Q^t_\kappa\,|I_c\rangle\, V^{c'c}_{\lambda\sigma\kappa}(r) . \tag{138}$$

The factor $G^{J\lambda\sigma\kappa}_{l's'j'c',lsjc}$ is a geometrical/statistical coefficient, which gives the appropriate weight to the angular momenta involved,

$$\begin{aligned}
G^{J\lambda\sigma\kappa}_{l's'j'c',lsjc} &= (-)^{J+I'_c+j}\, i^{l'+l+\lambda} \\
&\qquad\qquad \overline{\times \sqrt{(2l'+1)(2l+1)(2\lambda+1)(2j'+1)(2j+1)(2\mu+1)}} \\
&\times \begin{pmatrix} l' & l & \lambda \\ 0 & 0 & 0 \end{pmatrix} \begin{Bmatrix} j' & j & \kappa \\ I_c & I_{c'} & J \end{Bmatrix} \begin{Bmatrix} l' & l & \lambda \\ s' & s & \sigma \\ j' & j & \kappa \end{Bmatrix} .
\end{aligned} \tag{139}$$

The reduced matrix elements of the projectile and target angular momentum tensor operators, $\langle s'|\,Q^p_\sigma\,|s\rangle$ and $\langle I_{c'}|\,Q^t_\kappa\,|I_c\rangle$ can, in principle, contain information about the nuclear part of the matrix elements. In the macroscopic models discussed, the reduced matrix element for the projectile is just a number, the number 1, to be precise. The reduced matrix element for the target depend on the oscillation amplitude in the vibrational model and on the deformation parameters in the rotational one.

Models with quite general couplings can be constructed in terms of their reduced matrix elements and form factors. In this way, it is possible to construct microscopic as well as alternative macroscopic models of the nuclear coupling. ECIS95 permits the definition of the interaction in terms of its reduced matrix elements and form factors (the geometrical factor is calculated within the code). It thus has the flexibility to perform coupled-channels calculations with an almost arbitary coupling.

13 The ECIS method and the DWBA in ECIS95

When the spin-orbit potential is not deformed, there is almost no difference, from the user's point of view, between the conventional and ECIS methods of performing coupled-channels calculations in the code ECIS95. The information needed to perform the calculation is almost identical in

the two cases. The only differences are in technical details, such as the maximum number of ECIS iterations and the use or not of Padé approximants, and in the execution time, which is generally shorter when the ECIS method is used.

When the spin-orbit potential is deformed, the results of the conventional and the ECIS method of calculation can differ, as the conventional method cannot take into account the deivative terms that appear in the potential. Only the ECIS method can perform the calculation correctly in this case.

When compound-nucleus cross sections are requested from the code ECIS95, it is usually better to use the conventional method of calculation. To obtain the transmission coefficients, it is necessary to calculate the complete S-matrix. The conventional method of calculation is usually more efficient at doing this than the ECIS one (at least if the spin-orbit potential is not deformed).

The ECIS method in ECIS95 can always be used to calculate the first-order distorted-wave Born approximation. For this, the code must be restricted to perform just the first ECIS iteration. One must also take care that the excited states couple only to the ground state and not among themselves. From Eq. (122), it is clear that the ECIS method would take into account coupling among the excited states, if such coupling were included, thereby going beyond the DWBA.

A particular case of the second-order DWBA can also be performed using the ECIS method. In this case, which can be treated using a simple extension of the method above, the ground state couples to a set of excited states that couple to yet another set of distinct excited states. A direct coupling of the ground state to the second set of states could also be included. The states must be arranged so that the first set that couples to the ground state comes before the second set of excited states. Again, one must take care that no coupling is allowed among the states in each set. The ECIS method will then perform the second-order DWBA calculation in its first iteration, making it extremely useful for the calculation of two-step statistical direct cross sections.

14   Final remarks

These lectures have tried to describe the basic nuclear physics problems to which ECIS95 can be applied. For lack of time, however, only the most basic applications could be addressed. Several other possible applications, such as the more elaborate macroscopic models — the vibrational-rotational model and the asymmetric rotational model — as well as the Engelbrecht-Weidenmüller statistical model, were mentioned, but no details were given. Many of the capabilities of ECIS95 were not even mentioned. Among these are the ability to perform Dirac optical model calculations, heavy-ion optical model calculations that include long-range Coulomb excitation and excitation of both the projectile and the target, and calculations of transfer-reaction cross sections within the zero-range distorted-wave Born approximation. In short, the code ECIS95 has many capabilities. It can be a powerful tool in the hands of those who know how to use it.

The optical model and optical potential continue to be subjects of intense research. One

can find out more about the directions this research is taking in the proceedings of a recent conference[23].

Acknowledgments

References

[1] C.M. Perey, F.G. Perey, J.A. Harvey, N.W. Hill, N.M .Larson, R.L. Macklin,"^{58}Ni+n transmission, differential elastic scattering and capture measurements and analysis from 5 to 813 keV", ORNL-TM-10841, (1988); EXFOR file #12972003.

[2] A. Brusegan, G.Rohr, R.Shelley, E.Macavero, C. Van Der Vorst, F. Poortmans, I. Mewissen, and G. Vanpraet, "Very high resolution transmission measurements and resonance parameters of ^{58}Ni and ^{60}Ni"; EXFOR file #22314006.

[3] T.Ericson, Advances in Physics, Vol. IX, No. 36, 425 (1960).

[4] H. Feshbach, *Theoretical Nuclear Physics: Nuclear Reactions*, John Wiley and Sons, Inc., New York (1992).

[5] J.P. Delaroche, Ch. Lagrange, and J. Salvy, IAEA-190, Vol. 1, (Vienna, 1976), p. 251.

[6] J.P. Jeukenne, A. Lejeune, and C. Mahaux, Phys. Rev. **C16**, 80 (1977).

[7] C. Mahaux and R. Sartor, in *Proceedings of the Specialists' Meeting on the Use of the Optical Model for the Calculation of Neutron Cross Sections below 20 MeV*, OECD, Paris, (1986), p. 17.

[8] F. Osterfeld, in *Proceedings of the Specialists' Meeting on the Use of the Optical Model for the Calculation of Neutron Cross Sections below 20 MeV*, OECD, Paris, (1986), p. 29.

[9] B.D. Serot and J.D. Walecka, Adv. Nucl. Phys. **16** 1 (1986).

[10] R.J. Glauber, in *Lectures in Theoretical Physics*, Interscience, New York, (1959), Vol. 1, p. 315.

[11] A.K. Kerman, H. McManus, and R.M. Thaler, Ann. Phys. (N.Y.) **8**, 551 (1959).

[12] C. Mahaux and H. Ngô, Nucl. Phys. **A378**, 205 (1982).

[13] C. M. Perey and F. C. Perey, Nucl. Dat. Tab. **14**, 293 (1974).

[14] *Handbook for calculations of nuclear reaction data : Reference input parameter library*, IEAE-TECDOC-1034; See also http://www-nds.iaea.or.at.

[15] R. G. Newton, *Scattering Theory of Waves and Particles*, McGraw-Hill, Inc., New York (1966).

[16] A. Prince, in *Proceedings of the International Conference on Nuclear Data*, Antwerp, (1982).

[17] J. Raynal, "Optical model and coupled channel calculations in nuclear physics" in *Computing as a Language of Physics*, International Atomic Energy Agency, Vienna (1972).

[18] J. Raynal, "Strong channel coupling method for cross-section calculation", Workshop on Nuclear Model Computer Codes, Trieste, Italy (1984).

[19] J. Raynal, Notes on ECIS94 — Note CEA-N-2772 (1994).

[20] A. deShalit and H. Feshbach, *Theoretical Nuclear Physics Volume 1: Nuclear Structure*, John Wiley and Sons, Inc., New York (1974).

[21] P.G. Young, in *Handbook for calculations of nuclear reaction data: Reference input parameter library*, IEAE-TECDOC-1034, p.131.

[22] C. A. Engelbrecht and H. A. Weidenmüller, Phys. Rev. **C8**, 859 (1973).

[23] *Proceedings of the Specialists' Meeting on the Nucleon Nucleus Optical Model up to 200 MeV*, OECD, Bruyères-le-Chatel (1996).

Appendix A: A dialogue with the code PRECIS

The following is a sample dialogue with the code PRECIS. This particular example prepares the input file of Exercise 4, which will adjust the phonon amplitude of the vibrational model to a set of n+^{58}Ni differential and integrated cross sections.

```
To prepare an input file for ECIS95, begin by entering the name of your file.
ecis-ex4
Enter the title that you wish to appear on the output.
n + 58Ni  --  Optical parameters fit to data set
Enter 1 if the logical switches are to be printed
      0 otherwise.
1
Enter the number corresponding to the projectile.
                  1 - neutron
                  2 - proton
                  3 - deuteron
                  4 - tritium
                  5 - helium-3
                  6 - alpha
1
Enter the charge, mass, spin and parity (+1 or -1) of the target.
 28.  58.  0.  1.
Enter 1 to use a global potential,
      0 to enter the potential parameters.
0
Enter 1 if dispersion terms are to be taken into account,
      0 otherwise.
0
Enter r0(v), r1(v), av, v0, v1, v2, vl and cv,
where v = v0 + v1*e + v2*e**2 + vl*ln(e) + cv*sqrt(e) and rv0=r0(v) + r1(v)*e.
 1.27  0.  0.75  48.87 -0.369  0.002  0.  0.
Enter r0(ws), r1(ws), aws, ws0, ws1, ws2, wsl and cws,
where ws = ws0 + ws1*e + ws2*e**2 + wsl*ln(e) + cws*sqrt(e)
and rws0=r0(ws) + r1(ws)*e.
 1.34  0.  0.375  14.13  0.16 -0.006  0.  0.
Enter r0(w), r1(w), aw, w0, w1, w2, wl and cw,
where w = w0 + w1*e + w2*e**2 + wl*ln(e) + cw*sqrt(e) and rw0=r0(w) + r1(w)*e.
 1.2  0.  0.6  0.  0.  0.  0.  0.
Enter r0(vso), r1(vso), avso, vso0, vso1, vso2, vsoland cvso,
where vso=vso0 + vso1*e + vso2*e**2 + vsol*ln(e) + cvso*sqrt(e)
and rvso0=r0(vso) + r1(vso)*e.
```

```
 1.267  0.  0.75  6.75  0.  0.  0.  0.
Enter rc0 and ewmax.
 1.25  12.
For each of the potentials  vc, w, vso and wso, enter 1 if its deformation
is to be taken into account, otherwise enter 0.
0 0 0 0
Enter the number of excited states to be used.
1
Enter 0 to use the vibrational model,
      1 to use the rotational model.
0
Enter the number of distinct phonons to be used.
1
For each phonon, enter its angular momentum and its amplitude.
2  0.2
Enter the energy (in MeV), spin and parity (+1 ou -1) of the first
excited state.
 1.454  2.  1.
Enter the number of phonons used to describe the first
excited state.
1
Enter the number(s) identifying the phonon(s) used to describe this state
      phonon no.     1
               1     2
1
Enter 1 to include the contribution of the compound nucleus,
      0 otherwise.
0
Enter 1 to use the standard coupled channels method,
      0 to use the ECIS method.
1
Enter 1 if the C-matrix elements, C=(S-1)/2i, are to be printed
      0 otherwise.
1
Enter 1 if the transmission coefficients are to be written on unit7,
      0 otherwise.
1
Enter 1 if angular distributions are to be calculated,
      0 otherwise.
0
Enter 1 if experimental data are to be input,
```

0 otherwise.
1
Enter 1 if experimental angular distributions are to be plotted,
        0 otherwise.
0
Enter 1 if parameters are to be adjusted,
        0 otherwise.
1
For each of the following parameters, enter the precision desired of the fit.
If the precision is given as 0., the parameter will not be adjusted.
          v, rv0, av
 0.   0.   0.
          vs, rvs0, avs
 0.   0.   0.
          ws, rws0, aws
 0.   0.   0.
          w, rw0, aw
 0.   0.   0.
          vso, rvso0, avso
 0.   0.   0.
          wso, rwso0, awso
 0.   0.   0.
          The amplitude of the multipolarity 2 phonon
 0.01
Enter the number of projectile energies at which calculations will be performed.
7
Enter 1 if the experimental data are on file,
        0 if they will be input.
1
Enter the complete name of the data file.
ecis-ex4.dat
Enter 1 to prepare the input data to another ECIS95 calculation,
        0 to stop.
0
Your input to ECIS95 is in file ecis-ex4.in.

Appendix B: Computer Exercises

Introduction to the Code ECIS95

Date — 14-03-00

Exercise 1 — n + ^{58}Ni$_{28}$

1. Spherical Optical Model Calculation: Using the program PRECIS, generate an input data file for the ECIS95 code for neutrons incident on ^{58}Ni$_{28}$ at 0.1, 1.0 and 10.0 MeV in the laboratory system that:

   - Includes only the 0^+ ^{58}Ni ground state,
   - Uses the global optical potential parameters of Wilmore-Hodgson,
   - Prints the C-matrix elements, C=(S-1)/2i, and
   - Calculates and plots the differential elastic cross section in $10°$ intervals from $0°$ to $180°$.

   Look at the contents of the input data file and try to identify the parameters that you entered.

   If you have not requested that transmission coefficients be calculated, you should find only one output file from ECIS95. It contains the input data used, the C-matrix elements and integral and differential cross sections. For each value of the incident energy,

   - Find the optical potential parameters,

     – Find the C-matrix elements, and

     – Find the integral and differential cross sections.

Are the optical potential parameters constant?

Exercise 2 — p + ^{58}Ni$_{28}$

1. Spherical Optical Model Calculation: Using the program PRECIS, generate an input data file for the ECIS95 code for protons incident on ^{58}Ni$_{28}$ at 1.0 and 10.0 MeV in the laboratory system that:

   - Includes only the 0^+ ^{58}Ni ground state,
   - Uses the global optical potential parameters of Perey,
   - Prints the C-matrix elements, C=(S-1)/2i, and

42

- Calculates and plots the differential elastic cross section in $10°$ intervals from $10°$ to $180°$.

Look at the contents of the input data file and try to identify the parameters that you entered.

If you have not requested that transmission coefficients be calculated, you should find only one output file from ECIS95. It contains the input data used, the C-matrix elements and integral and differential cross sections. For each value of the incident energy,

- Find the optical potential parameters,

  - Find the C-matrix elements, and
  - Find the integral and differential cross sections.

Are the optical potential parameters constant? What happened to the integral cross sections? Why didn't you do this calculation at 0.1 MeV?

Exercise 3 — n + $^{58}\mathrm{Ni}_{28}$

1. Spherical Optical Model Calculation: Using the program PRECIS, generate an input data file for the ECIS95 code for neutrons incident on $^{58}\mathrm{Ni}_{28}$ that:

   - Includes only the 0^+ $^{58}\mathrm{Ni}$ ground state,

   - Uses the following optical potential parameters:

     - $r_V = 1.27$ fm, $a_V = 0.75$ fm, $V_0 = 48.87$ MeV, $V_0 = -0.369$, and $V_2 = 0.002$ MeV^{-1},

     - $r_{W_s} = 1.34$ fm, $a_{W_s} = 0.375$ fm, $W_{s0} = 14.3$ MeV, $W_{s1} = 0.16$, $W_{s2} = -0.006$ MeV^{-1},

     - $r_{V_{so}} = 1.27$ fm, $a_{V_{so}} = 0.75$ fm, and $V_{so0} = 6.75$ MeV,

     with all other potential strengths zero,

   - Includes the file of experimental data ecis-ex3.dat,

   - And adjusts the diffusivity a_{W_s} of the surface imaginary potential.

Look at the contents of the input data file and try to identify the parameters that you entered.

- Find the final values of the adjusted parameter.

- Find the comparisons between the experimental data and the calculations.

How would you use your results?

Exercise 4 — n + ^{58}Ni$_{28}$

1. Deformed Optical Model Calculation: Using the program PRECIS, generate an input data file for the ECIS95 code for neutrons incident on ^{58}Ni$_{28}$ that:

   - Includes the 0^+ ^{58}Ni ground state and the 2^+ excited state at 1.454 MeV as a vibrational state,

   - Uses the following optical potential parameters:

     - $r_V = 1.27$ fm, $a_V = 0.75$ fm, $V_0 = 48.87$ MeV, $V_0 = -0.369$, and $V_2 = 0.002$ MeV^{-1},

     - $r_{W_s} = 1.34$ fm, $a_{W_s} = 0.375$ fm, $W_{s0} = 14.3$ MeV, $W_{s1} = 0.16$, $W_{s2} = -0.006$ MeV^{-1},

     - $r_{V_{so}} = 1.27$ fm, $a_{V_{so}} = 0.75$ fm, and $V_{so0} = 6.75$ MeV,

     with a phonon amplitude $\beta_2 = 0.2$ and all other potential strengths zero,

   - Uses the standard coupled-channels method,

   - Includes the file of experimental data ecis-ex4.dat,

   - And adjusts the phonon amplitude $\beta_2 = 0.2$.

   Look at the contents of the input data file and try to identify the parameters that you entered.

   - Find the final values of the adjusted parameter.

   - Find the comparisons between the experimental data and the calculations.

How do the inelastic cross sections vary with energy? How do the the reaction cross sections and differential elastic cross sections compare with the those you obtained with the spherical optical model? How would you use your results?

Exercise 5 — n + ^{58}Ni$_{28}$

1. Deformed Optical Model Calculation: Using the program PRECIS, generate an input data file for the ECIS95 code for neutrons incident on ^{58}Ni$_{28}$ in the range of energy from 0.1 MeV to 20 MeV in the laboratory system that:

   - Includes the 0^+ ^{58}Fe ground state and the 2^+ excited state at 1.454 MeV as a vibrational state,

- Uses the following optical potential parameters:

  - $r_V = 1.27$ fm, $a_V = 0.75$ fm, $V_0 = 48.87$ MeV, $V_0 = -0.369$, and $V_2 = 0.002$ $\mathrm{MeV^{-1}}$,

  - $r_{W_s} = 1.34$ fm, $a_{W_s} = 0.375$ fm, $W_{s0} = 14.3$ MeV, $W_{s1} = 0.16$, $W_{s2} = -0.006$ $\mathrm{MeV^{-1}}$,

  - $r_{V_{so}} = 1.27$ fm, $a_{V_{so}} = 0.75$ fm, and $V_{so0} = 6.75$ MeV,

  with a phonon amplitude $\beta_2 = 0.2$ and all other potential strengths zero,

- Uses the standard coupled-channels method,

- Prints the C-matrix elements, C=(S-1)/2i,

- Calculates transmission coefficients.

Look at the contents of the input data file and try to identify the parameters that you entered.

After running ECIS95, you should find two output files. One of these contains the input data used, the C-matrix elements and integral and differential cross sections. The other will contain the transmission coefficients. Studying these, for each value of the incident energy,

- Find the optical potential parameters,

  - Find the C-matrix elements,

  - Decipher the file of transmission coefficients. In what order are they listed?

How do these quantities vary with energy?

Exercise 6 — n + $^{238}\mathrm{U}_{92}$

1. Deformed Optical Model Calculation: Using the program PRECIS, generate an input data file for the ECIS95 code for neutrons incident on $^{238}\mathrm{U}_{92}$ at 0.1, 1.0 and 10.0 MeV in the laboratory system that:

   - Includes the 0^+ $^{238}\mathrm{U}$ ground state and the excited rotational 2^+ state at 0.044 MeV and 4^+ state at 0.148 MeV,

   - Uses the global optical potential parameters of Madland and Young and static deformations $\beta_2 = 0.198$ and $\beta_4 = 0.057$,

   - Uses the standard coupled-channels method,

   - Prints the C-matrix elements, C=(S-1)/2i,

   - Calculates and plots the differential cross sections in 10° intervals from 0° to 180°, and

- Calculates transmission coefficients.

Once the input data file is prepared, look at its contents and try to identify the parameters that you entered.

After running ECIS95, you should find two output files. One of these contains the input data used, the C-matrix elements and integral and differential cross sections. The other will contain the transmission coefficients. Studying these, for each value of the incident energy,

- Find the optical potential parameters,

  - Find the C-matrix elements,
  - Find the integral and differential cross sections for the elastic and inelastic channels, and
  - Decipher the file of transmission coefficients. In what order are they listed?

How do these quantities vary with energy? How do they compare with the results you obtained with the vibrational model?